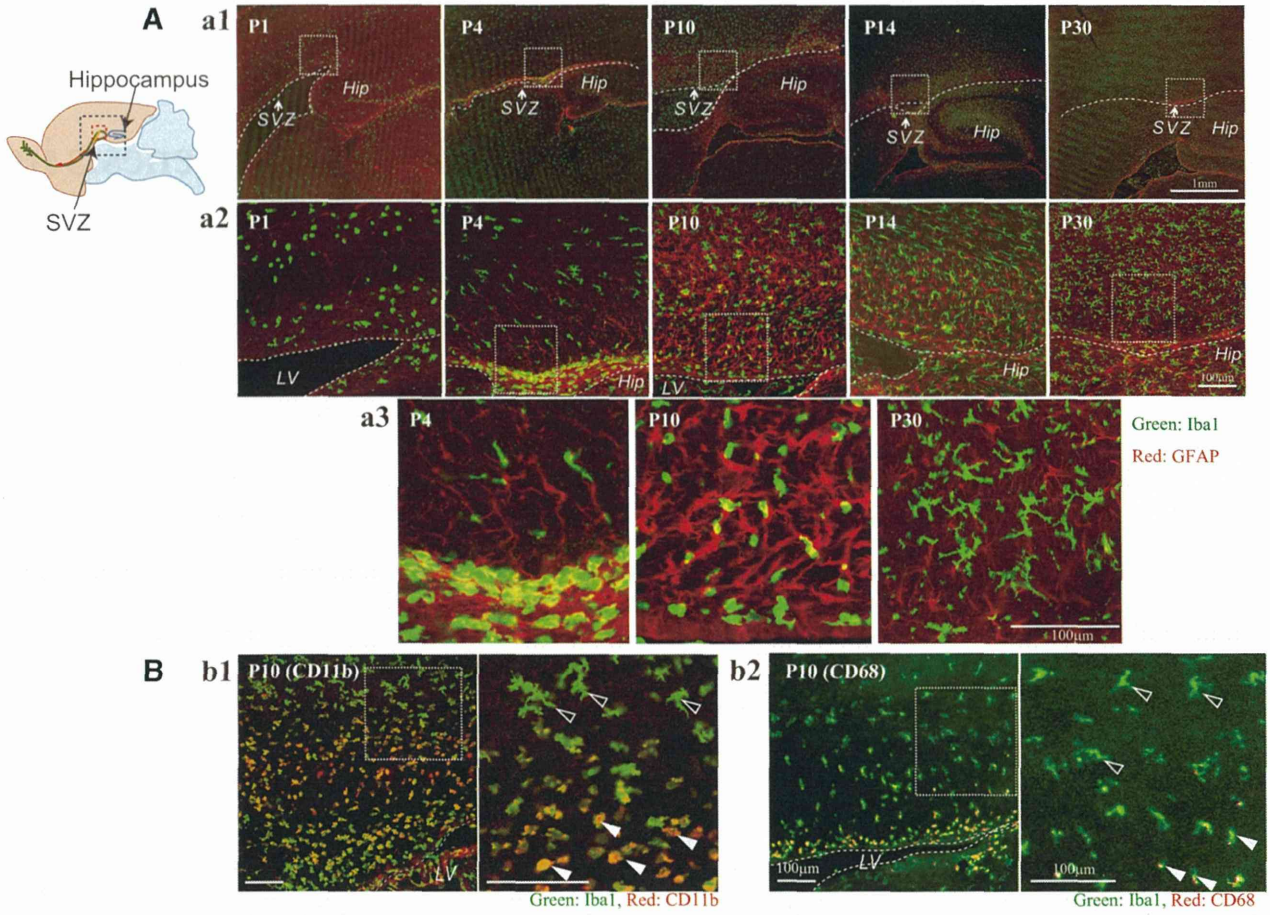

Figure 1. There is a population of activated microglia accumulated in the early postnatal SVZ. ***Aa1***, Distribution of microglia in the postnatal VZ/SVZ (P1, P4, P10, P14, P30). Sagittal sections of forebrains were immunostained with anti-Iba1 (green: microglia) and anti-GFAP antibodies (red: neural stem cells and astrocytes). ***Aa2***, Magnified images of the hatched squares in ***Aa1***. The accumulation in the SVZ in P4 and P10 was distinctive. ***Aa3***, Magnified images of the hatched squares in ***Aa2***. Morphological changes of microglia with age from amoeboid shape to more ramified shape is remarkable (P4, P10, P30). ***Bb1***, Activation of microglia in P10 SVZ. Sagittal sections immunostained with anti-CD11b (red: activated microglia) and anti-Iba1 antibodies (green: microglia). Right panel, Magnified image of the hatched square in the left panel. The microglia in the SVZ have an amoeboid shape and positive for CD11b (white arrowheads), whereas those outside SVZ have more ramified shape and are negative for CD11b (black arrowheads). ***Bb2***, Sagittal sections immunostained with anti-CD68 (red: activated microglia) and anti-Iba1 antibodies (green: microglia). Right panel, Magnified image of the hatched square in the left panel. The microglia in the SVZ have an amoeboid shape and positive for CD68 (white arrowheads), whereas those outside SVZ have more ramified shape and are negative for CD68 (black arrowheads). Similar results were obtained in three independent experiments.

access to food and water. Minocycline (30 mg/kg) or the same volume of PBS was injected into rats of either sex intraperitoneally for 3 d from postnatal day 2 (P2). Six hours after the last injection, rats were deeply anesthetized and the brains were removed on ice.

Immunohistochemistry (sagittal sections). Rats (P1, P4, P10, P14, P30) were anesthetized and then perfused with saline followed by 4% PFA, and then the brains were removed. From each half brain, sagittal sections were cut laterally at a thickness of 30 μm beginning 2 mm lateral from the midline. The sections were incubated for 2 h at room temperature in a blocking solution (3% normal goat serum, 0.3% Triton X-100 in PBS) and incubated for 24 h at 4°C in the solution, including the primary antibodies (rabbit anti-Iba1 antibody [019–9741, Wako; 1:500], mouse anti-GFAP antibody [MAB3402, Millipore; 1:200], mouse anti-rat CD11b antibody [MAB1405, AbD Serotec; 1:100], anti-rat CD68 antibody [MCA341R, AbD Serotec; 1:100], rabbit anti-Ki-67 [SP6, M3061, Spring Bioscience; 1:10], anti-nestin antibody [MAB353, Millipore; 1:100], goat anti-doublecortin [Dcx] antibody [sc-8066, Santa Cruz Biotechnology; 1:200], goat anti-PDGFRα antibody [sc-31178, Santa Cruz Biotechnology; 1:50], anti-oligodendrocyte marker O1 [O1] antibody [MAB344, Millipore, 1:50], mouse anti-MBP antibody [MAB 382, Millipore; 1:50], rabbit anti-ALDH1L1 antibody-astrocyte marker antibody [ab87117, Abcam; 1:1000], mouse anti-S100β antibody [S2532, Sigma; 1:100], rabbit anti IGF-1 antiserum [GroPep Biotechnology; [1:200]). After incubation, the sections were washed and incubated for 3 h at room temperature in the solution, including the secondary antibodies (anti-rabbit IgG-conjugated Alexa Fluorochrome or anti-mouse IgG-conjugated Alexa Fluorochrome [Invitrogen; 1:1000]). The stained sections were analyzed using a Nikon A1R-A1 confocal microscope system. To count the number of cells positive for each differentiation marker, 613 × 613 μm^2 and 1024 × 1024 μm^2 squares were set on both sides of the fornix. The cell numbers in the two squares were counted and averaged for the cell numbers in one section. The averaged data of 3 sections at 90 μm intervals were treated as the data of one animal and the data from 6 animals were statistically analyzed.

Immunohistochemistry (coronal sections). Three points on the skull at three different rostrocaudal stereotaxic coordinates (i.e., anterior, middle, posterior) were marked with animal tattoo ink (Ketchum) at P1. These three points with different rostrocaudal levels were determined according to a previous report (Suzuki and Goldman, 2003): rostral point: 2 mm anterior, 1 mm lateral to the bregma; middle point: 0.7 mm anterior, 1 mm lateral to the bregma; caudal point: 0.5 mm posterior, 1 mm lateral to the bregma. Then the animals were perfused at P1, P3, P10, and P30, and the brains were removed as described above. From each half brain, coronal sections were cut at each marked point from anterior to posterior. The sections were immunostained with anti-Iba1 and anti-CD68 as described above. After immunostaining, the sections were coun-

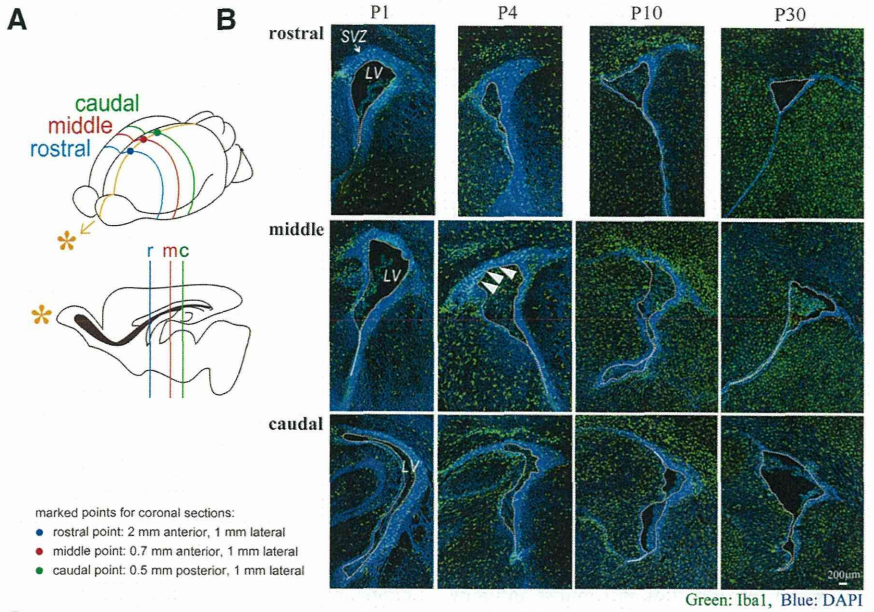
A
B
caudal
middle
rostral
r mc
P1
P4
P10
P30
rostral
middle
caudal
SVZ
LV
marked points for coronal sections:
rostral point: 2 mm anterior, 1 mm lateral
middle point: 0.7 mm anterior, 1 mm lateral
caudal point: 0.5 mm posterior, 1 mm lateral
200μm
Green: Iba1, Blue: DAPI

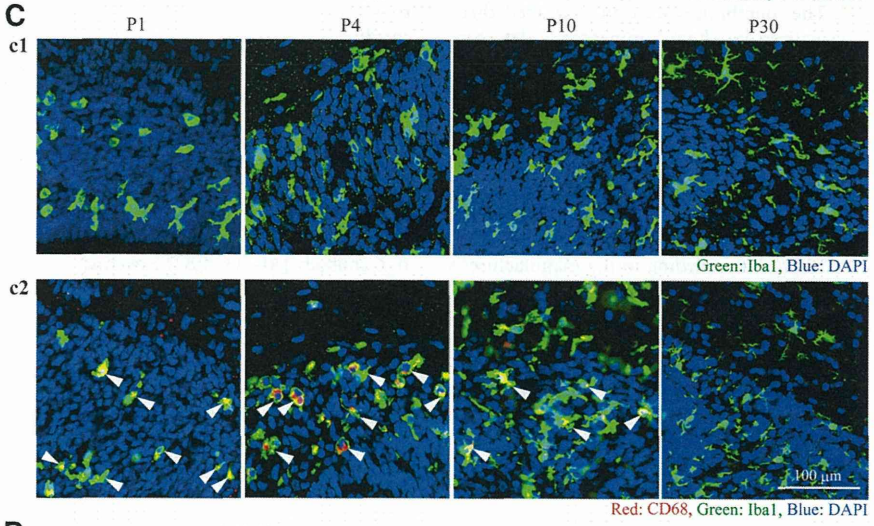
C
c1
c2
P1
P4
P10
P30
Green: Iba1, Blue: DAPI
100 μm
Red: CD68, Green: Iba1, Blue: DAPI

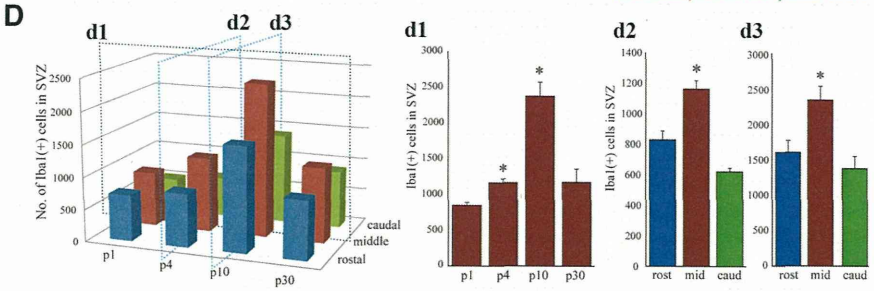
D
d1
d2
d3
No. of Iba1(+) cells in SVZ
p1
p4
p10
p30
caudal
middle
rostral
Iba1(+) cells in SVZ
rost
mid
caud

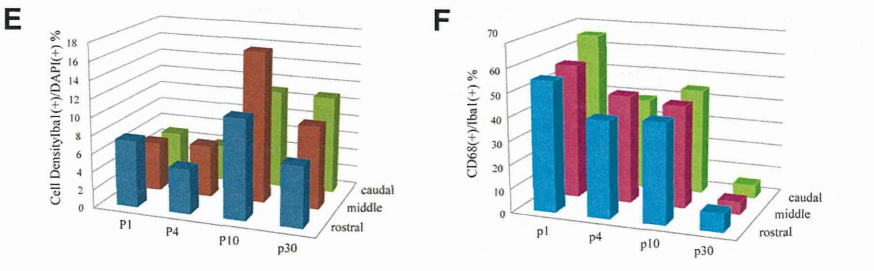
E
F
Cell Density(Iba1(+)/DAPI(+) %
CD68(+)/Iba1(+) %
P1
P4
P10
p30
caudal
middle
rostral

terstained with DAPI (1:500; Invitrogen) for 30 min to visualize the SVZ. The cell numbers of microglia (Iba1 $^+$) and activated microglia (Iba1 $^+$ CD68 $^+$) in the SVZ (the region with dense DAPI signals) were counted in one section. The averaged data of three sections at 90 μm intervals across the marked points were treated as the data for each rostrocaudal level. The data from 6 to 9 hemispheres per one rostrocaudal level were statistically analyzed.

Western blotting. P4 Wistar rat brains were cut into sagittal sections. Under a microscope, a parasagittal section (from 1 mm lateral, 2 mm thickness) was taken from each half brain and meninges were carefully removed. The VZ/SVZ was identified by its slightly darker, more transparent appearance compared with the overlying corpus callosum. We cut out the VZ/SVZ between 0.4 mm anterior and 3 mm posterior (posterior end of SVZ) from bregma so as not to include the rostral migratory stream. Dissected VZ/SVZ tissues were homogenized on ice in extraction buffer (20 mM Tris, 2 mM EDTA, 0.5 mM EGTA, 0.32 M sucrose, protease inhibitor mixture), and centrifuged at 1000 × *g* for 10 min. Proteins in the lysates were resolved with SDS-PAGE and transferred to PVDF membranes. The membranes were incubated overnight in BlockAce blocking solution at 4°C. Then the membranes were incubated with primary antibodies (anti-CD11b [1:1000], anti-CD68 [1:2000], anti-nestin [1:1000], anti-PDGFRα [1:200], anti-ALDH1L1 [1:1000], anti-S100β [1:2000]) for 1 h at 25°C. After washing three times, the membranes were incubated with HRP-conjugated anti-rabbit or anti-mouse antibody (1:5000) for 1 h at 25°C. The membranes were then washed three times and signals were visualized by chemiluminescence detectors LAS3000 (Fuji film).

Measurement of cytokine levels. Cytokine levels in the SVZ were determined with Bio-Plex cytokine analysis system (Bio-Rad Laboratories). Tissue lysates of VZ/SVZ fractions were obtained from rats at P1, P4, P10, and P30 as described in Western blotting. The concentrations of Il-1α, Il-1β, IL-2, IL-4, IL-6, Il-10, GM-CSF, IFN-γ, and TNF-α were measured by the Bio-Plex rat cytokine 9 plex kit according to the manufacturer's instruction. In some cases, IGF-1, Il-1β IL-6, TNF-α, and IFN-γ concentrations were measured by ELISA kit according to the manufacturer's instruction. The protein levels of tissue lysates were measured by BCA protein assay. The amount of each cytokine in 100 μg of total protein is shown for comparison. To determine the cytokine release from activated microglia *in vitro*, microglia were activated by LPS (10 ng/ml) in the presence or absence of minocycline (10 μM) for 30 min and washed carefully and incubated in the normal medium for 24 h. After 24 h incubation, the cell culture supernatants were collected, and concentration of Il-1β, IL-6, IFN-γ, and TNF-α were measured by ELISA kit.

Cell culture: neurosphere culture. Rat neural stem cells were cultured as previously described (Reynolds et al., 1992; Hamanoue et al., 2009) with slight modifications. Briefly, telencephalons were dissected from embryonic day 16 (E16) rats of either sex in ice-cold DMEM/F12, minced, and dispersed into single cells by pipetting. Cells were then cultured in DMEM/F12 containing B27 supplement (×200), 20 ng/ml FGF2, and 20 ng/ml EGF for 7 d. The primary neurospheres and single cells were differentiated in growth factor-free medium in glass chambers coated with ornithine/fibronectin. In some cases, primary neurosphere were incubated with TrypLE Select for 15 min and dissociated by pipetting. Single cells were differentiated in glass chambers coated with polyornithine/laminin.

Microglia culture. Rat microglia were cultured as previously described (Nakajima et al., 1992). In brief, mixed glial cultures were prepared from the cerebral cortex of P1 Wistar rats and maintained for 12–23 d in DMEM containing 10% FBS. The floating microglia over the mixed glial cultures were collected and transferred to appropriate dishes or transwells.

Neural stem cell differentiation assay. To examine the effects of activated microglia on neural development and the contribution of cytokines to the effects, we used modified cocultures of neurospheres with activated microglia. Microglia cultured independently of neurospheres on transwells were activated by LPS (10 ng/ml) in the presence or absence of minocycline (10 μM) for 30 min and washed carefully to prevent residual LPS and minocycline. The transwells on which microglia were cultured were set on the neurospheres 1 d after the starting point of the differentiation and incubated for differentiation periods suitable for neurons (7 d) or oligodendrocytes (11 d). In some cases, we performed the coculture of cells dissociated from neurospheres and activated microglia. To check the effects of minocycline alone, these cells were incubated in the presence of minocycline (10 μM) for 7 d. Neurospheres and single neural stem cells were immunohistochemically stained for β3-tubulin, PDGFRα, O4, GFAP, and TOTO3 according to the manufacture's instruction (Stem Cell Kits, R&D Systems). To examine the effects of function-blocking antibodies on differentiation, the neurospheres were differentiated in the presence of function-blocking antibodies (goat anti-rat IL-1β antibody [AF-501-NA, R&D Systems], goat anti-rat IL-6 antibody [AF-506, R&D Systems], TNF-α antibody [70R-TR007X, Fitzgerald], and goat anti-mouse/rat IFN-γ antibody [AF-585-NA, R&D Systems]) (1 μg/ml for each). The effects of these function-blocking antibodies were compared with the same concentration of isotype-matched control IgG: normal goat IgG control [AB-108-C, R&D Systems] and rabbit IgG control [31R-AR001, R&D Systems] (1 μg/ml for each). The effect of the mixture of function blocking antibodies (goat anti-rat IL-1β antibody, goat anti-rat IL-6 antibody, TNF-α antibody, and goat anti-mouse/rat IFN-γ antibody, 1 μg/ml for each) was compared with the control, which included same concentrations of isotype-matched control IgGs (i.e., 3 μg/ml of normal goat IgG control and 1 μg/ml of rabbit IgG control). To examine the effects of a single cytokine, the neurospheres were differentiated in the presence of each individual recombinant cytokine (rIL-1β, rIL-6, rTNF-α, and rIFN-γ at 1 or 10 ng/ml). After the differentiation period, the cells were stained immunocytochemically as described above.

Data analysis and statistics. All data are shown as the mean ± SEM. Statistical analysis was performed using Student's *t* test, or Tukey's test by ANOVA. Differences were considered to be significant at $p < 0.05$.

Materials. Minocycline, LPS, anti-S100β antibody (S2532), and EGF were purchased from Sigma. Bio-Plex rat cytokine 9 plex was purchased from Bio-Rad Laboratories. Recombinant cytokines (rIL-1β, rIL-4, rIL-6, rIFN-γ, rTNF-α) and FGF2 were purchased from PeproTech. Maximum sensitivity substrate and BCA protein assay were purchased from Thermo Scientific. CanGet Signals was purchased from Toyobo. HRP-conjugated anti-rabbit, mouse antibodies were purchased from GE Healthcare Life Science. DAPI, TOTO3, anti-mouse, sheep, rabbit IgG, and anti-mouse IgM-conjugated AlexaFluor were purchased from Invitrogen. BlockAce was purchased from DS Pharma Biomedical. B27 supplement, TrypLE Serect, FBS, and DMEM were purchased from Invitrogen.

Results

We first investigated the distribution of microglia in the postnatal rat forebrain (Figs. 1 and 2). Sagittal sections were immuno-

←

Figure 2. The temporal and spatial dynamics of activated microglia in the postnatal SVZ. ***A***, A schematic of the rostrocaudal levels in this experiment. ***B***, The distribution of microglia in the rostral, medial, and caudal SVZ at P1, P4, P10, and P30. Coronal sections of forebrains at rostral (2 mm anterior to the bregma), medial (0.7 mm anterior to the bregma), and caudal (0.5 mm posterior to the bregma) levels were immunostained with anti-Iba1 (green: microglia) followed by DAPI staining (blue: cell nuclei). A population of activated microglia accumulated within the SVZ at P1-P10. ***Cc1***, Typical morphology of microglia in the middle SVZ at P1, P4, P10, and P30. Morphological change of microglia with age from amoeboid shape to more ramified shape is remarkable. ***Cc2***, The middle SVZ sections immunostained with anti-CD68 (red: activated microglia) and anti-Iba1 antibodies (green: microglia). The microglia at P1, P4, and P10 in the SVZ have an amoeboid shape and are positive for CD68 (representative cells: white arrowheads), whereas those at p30 have a more ramified shape and are negative for CD68. ***D***, The quantification of the number of Iba1 $^+$ cells in the SVZ. ***d1***, Time course of the Iba1 $^+$ microglia in the middle SVZ. The number peaked at P10. d2, d3, The comparison of the numbers of microglia among the rostral, middle, and caudal SVZ at P4 (***d2***) and P10 (***d3***). *$p < 0.05$ versus p1 or rost group (Tukey's test by ANOVA). Data are mean ± SEM. ***E***, The cell density of Iba1 $^+$ microglia at different rostrocaudal levels at P1, P4, P10, and P30. The cell density of microglia in the SVZ paralleled with that of the number of microglia throughout a period of the observation. ***F***, The ratio of activated microglia in the SVZ (CD68 $^+$/Iba1 $^+$). During the experimental period, the highest ratio was obtained at P1. We confirmed the similar results in three independent experiments.

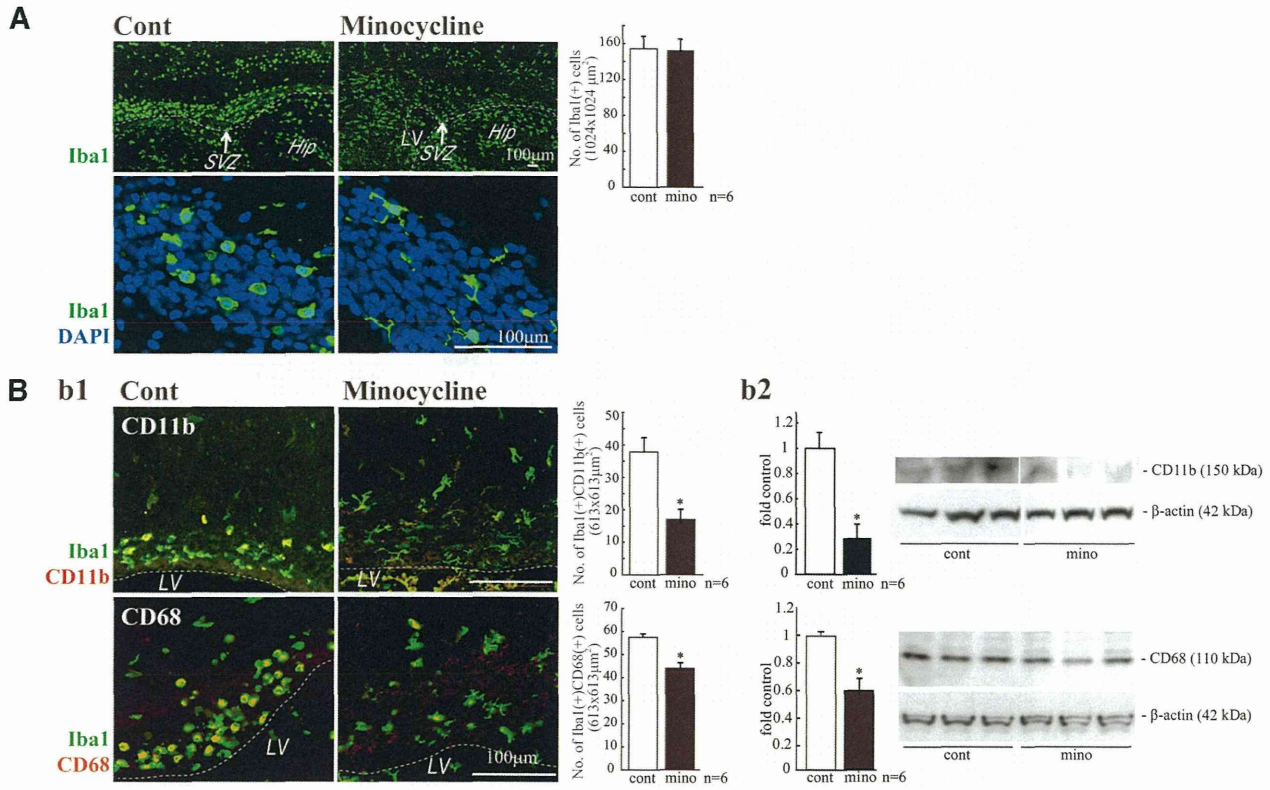

Figure 3. Minocycline suppressed microglial activation *in vivo*. ***A***, Effects of minocycline on the number of Iba1$^+$ cells in the SVZ and their morphologies. Minocycline was administered by intraperitoneal injection for 3 d beginning at P2 (30 mg/kg/d, P2-P4, $n = 6$/group). Sagittal sections of minocycline-treated forebrains were immunostained for Iba1 (green) followed by DAPI staining (cyan). Although the number of Iba1$^+$ microglia in the SVZ did not change (graph), their shape shifted from an amoeboid type to a more ramified type by minocycline (bottom). ***Bb1***, Effects of minocycline on the expression of activation markers and the morphologies of microglia. Sagittal sections of minocycline-treated forebrains were immunostained for Iba1 (green), and CD11b (red), and CD68 (red). Minocycline significantly decreased the number of cells positive for CD11b or CD68. The morphologies of the cells were also changed from amoeboid shape to more ramified shape. ***Bb2***, The significant decrease in the expression of CD11b and CD68 was confirmed by Western blotting of the SVZ as well. *$p < 0.05$ (Student's t test). Data are mean ± SEM. Similar results were obtained in three independent experiments.

stained with anti-Iba1, the marker for all microglia (green: microglia), and anti-GFAP antibodies (red: neural stem cells and astrocytes) at P1, P4, P10, P14, and P30. We found that a large number of microglia accumulated in the postnatal SVZ from P1 to P10 (Fig. 1*A*), especially at P4. The microglia in the VZ/SVZ at P1 and P4 display an amoeboid shape, whereas those outside the SVZ have a more ramified shape (Fig. 1*Aa2*). At P10, the number of microglia outside the SVZ had dramatically increased; the microglia in the VZ/SVZ remained amoeboid. At P14, the number of microglia had increased further and now ramified microglia were also observed in the VZ/SVZ. At P30, the numbers of microglia in the SVZ had decreased and most of the microglia had assumed a ramified shape. Further magnified images in Figure 1*Aa3* show that the shape of microglia in the SVZ changed gradually from amoeboid (P4) to ramified (P30). Figure 1*B* shows the expression of CD11b (Fig. 1*Bb1*) and CD68 (Fig. 1*Bb2*) in the SVZ microglia at P10. CD11b is potentially a marker for all microglia; however, its level is highly elevated by activation. CD68 is a marker for activated microglia. The levels of CD11b and CD68 are much higher in the amoeboid microglia in the SVZ (white arrowheads) than in the ramified ones outside the SVZ (black arrowheads), indicating that the SVZ amoeboid microglia have an activated phenotype.

To examine the developmental dynamics of microglia in the SVZ temporally and spatially, we examined the distribution of microglia in coronal sections that include rostral, medial, and caudal SVZ at P1, P4, P10, and P30 (Fig. 2). Each rostrocaudal level was determined according to a previous report (Suzuki and Goldman, 2003). Coronal sections were immunostained with anti-Iba1 (green: microglia) followed by DAPI staining (blue: cell nuclei) (Fig. 2*B*,*C*). The SVZ could be clearly delineated by its dense cellularity. From P1 to P10, a large number of microglia accumulated at all rostral, middle, and caudal levels. When we quantified the number of microglia in the SVZ, they gradually increased from P1 to P10, reached a maximum at p10, and decreased at P30 at all coronal levels (Fig. 2*B*,*D*, d1). Microglia displayed an amoeboid shape at P1, P4, and P10 but had become more ramified at P30 (Fig. 2*Cc1*). Among the different rostrocaudal levels, the number of microglia in the middle SVZ was significantly larger than in other levels at all ages (Fig. 2*D*, d2, d3). The changes in cell density (i.e., the ratio of Iba1$^+$/DAPI$^+$) of microglia in the SVZ paralleled that of the number of microglia throughout the period of observation (Fig. 2*E*). We next examined immunostaining for CD68 in SVZ microglia. Figure 2*Cc2* shows representative images of double staining with anti-Iba1 and anti-CD68. At P1 and P4, most Iba1+ microglia in the SVZ were also positive for CD68. At P4, the CD68 signals became much stronger. At P10, a few microglia had appeared that had little CD68. At P30, double-positive cells were markedly decreased in number. The time course of the ratio of CD68$^+$/Iba1$^+$ cells is shown in Figure 2*F*: the highest ratio was obtained at P1. The ratios at P4 and P10 were almost equivalent and then were

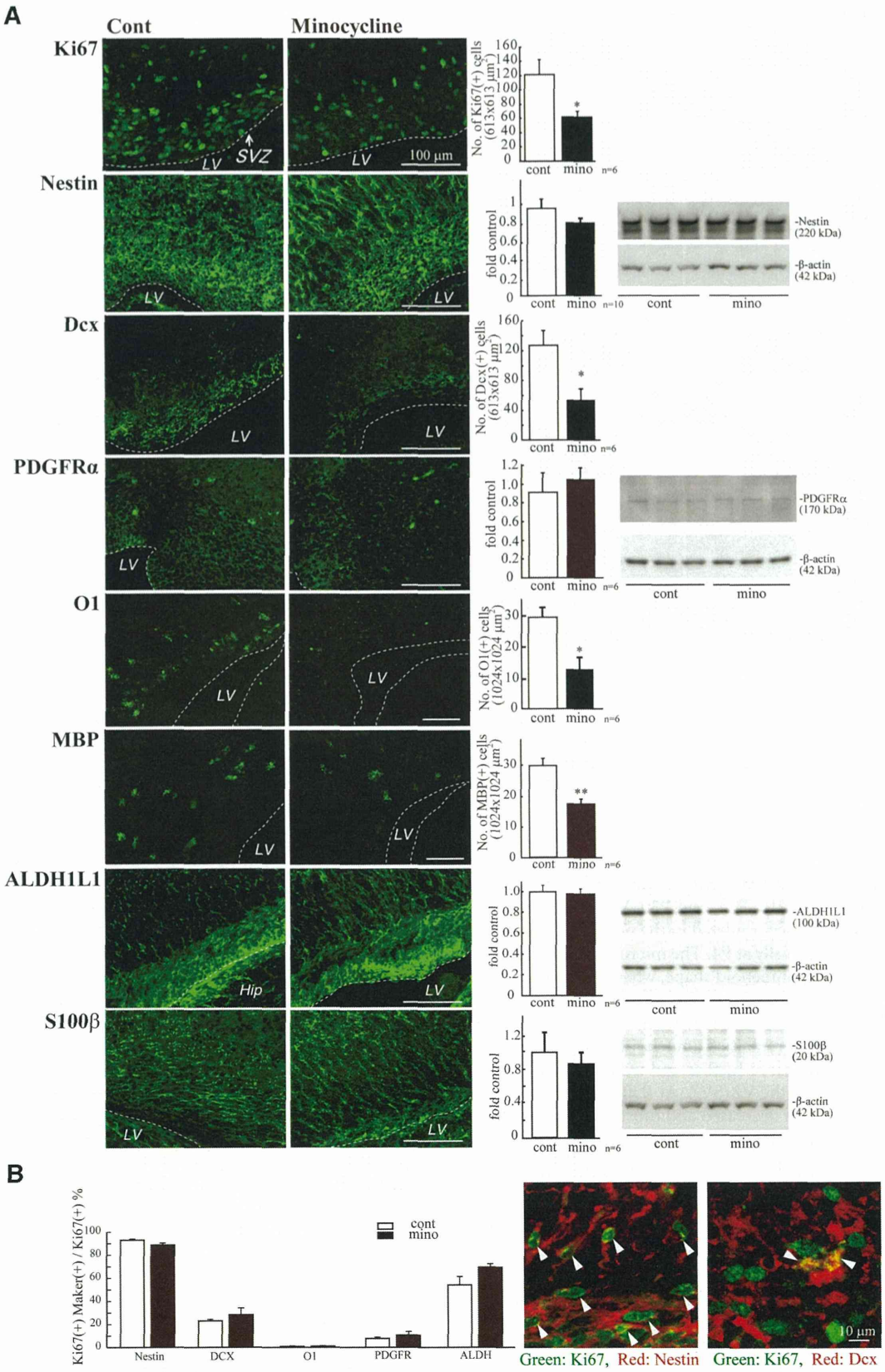

Figure 4. Minocycline decreased the numbers of proliferating cells, neuronal progenitors, and oligodendrocyte progenitors in the early postnatal SVZ. ***A***, Minocycline was administered by intraperitoneal injection for 3 d beginning at P2 (30 mg/kg/d, P2-P4, $n = 6$/group). Sagittal sections of forebrains were immunostained with antibodies to Ki67, nestin, Dcx, PDGFRα, O1, MBP, ALDH1L1, and S100β. The numbers of cells positive for Ki67, Dcx, MBP, or O1 were counted, whereas the protein levels of nestin, PDGFRα, ALDH1L1, and S100β (*Figure legend continues.*)

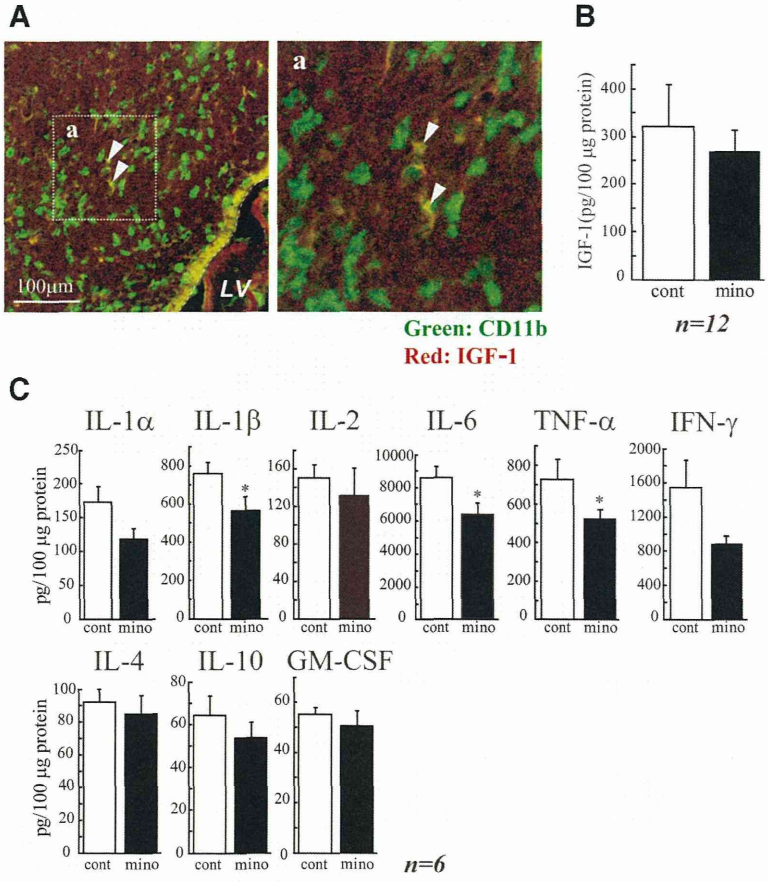

Figure 5. The activated microglia raised the cytokine levels in the SVZ. ***A***, A subpopulation of the microglia express IGF-1 in the early postnatal SVZ, but IGF-1 is not involved in the action of activated microglia during this period. Sagittal sections were immunostained with anti-CD11b (green: microglia) and anti IGF-1 (red) antibodies. Right panel, Magnified image of the square in the left. A subpopulation of microglia is positive for IGF-1 (arrowheads). The percentage of CD11b $^+$IGF-1 $^+$ was 43.42 ± 6.72% in CD11b $^+$ cells. ***B***, Minocycline did not affect the amount of IGF-1 in the early postnatal SVZ. Minocycline was administered by intraperitoneal injection for 3 d beginning at P2 (30 mg/kg/d, P2-P4, n = 6/group), and the amount of IGF-1 in the SVZ was quantified by ELISA. ***C***, Minocycline decreased the amount of inflammatory cytokines in the SVZ. IL-1α, IL-1β, IL-2, IL-4, IL-6, IL-10, GM-CSF, IFN-γ, and TNF-α levels in the SVZ tissue lysate were measured by BioPlex cytokine detection assay system. *$p <$ 0.05 (Student's t test). n = 6 rats/group. Data are mean ± SEM. Similar results were obtained in two independent experiments.

remarkably decreased at P30. These results are consistent with those obtained from the sagittal sections (Fig. 1), showing the population of activated microglia that accumulated within the SVZ during the early postnatal period.

We therefore examined the specific roles of these microglia in the early postnatal SVZ. At early postnatal ages, both neurogenesis and gliogenesis are active in the SVZ (Gould et al., 1999; Wagner et al., 1999; Doetsch and Scharff, 2001; Zerlin et al., 2004; Marshall et al., 2008). To suppress the activation of microglia, we used minocycline, a tetracycline antibiotic, long used to suppress microglial activation (Tikka et al., 2001; Zhao et al., 2007). We first verified the effects of minocycline on the activation of microglia. Minocycline was administered by intraperitoneal injection for 3 d beginning at P2 (30 mg/kg/d, P2-P4, n = 6/group), and sagittal sections of minocycline-treated rat forebrains were immunostained for Iba1, CD11b, and CD68. Minocycline did not change the numbers of Iba1-positive microglia in the VZ/SVZ (Fig. 3*A*, top), but it dramatically changed their shape from amoeboid to more ramified (Fig. 3*A*, bottom). The number of CD11b $^+$ cells was significantly decreased (Fig. 3*Bb1*, top and graph), and the decrease in CD11b levels in the SVZ was confirmed by Western blotting (Fig. 3*Bb2*, top graph and photo). The number of CD68 $^+$ cells and the level of CD68 were also decreased (Fig. 3*B*, bottom data). These results indicate that our administration of minocycline suppresses the activation of SVZ microglia.

We then investigated the effects of minocycline on early postnatal differentiation. After the administration of minocycline, sagittal sections were immunostained with differentiation markers: Ki67 (proliferating cells), nestin (stem cells), Dcx (neuronal progenitors), PDGFRα (oligodendrocyte progenitors [polydendrocytes]), O1 (oligodendrocyte progenitors [premyelinating oligodendrocytes]), MBP (mature oligodendrocyte [premyelinating and myelinating oligodendrocytes] (Nishiyama et al., 2009), ALDH1L1 (astrocyte progenitors), and S100β $^+$ (astrocytes) (Fig. 4*A*). The numbers of cells positive for Ki67, Dcx, O1, and MBP were counted, whereas the levels of nestin, PDGFα, ALDH1L1, and S100β were examined by Western blotting because it was hard to discriminate the cell morphologies by these signals. Minocycline significantly decreased the number of Ki67 $^+$ cells and slightly decreased the level of nestin. The number of cells positive for Dcx was also significantly reduced. Furthermore, minocycline decreased the numbers of cells positive for O1 and MBP, whereas the numbers of PDGFRα $^+$ cells rather tended to increase. The levels of ALDH1L1 and S100β did not change. These results suggest that activated microglia in the early postnatal SVZ enhance neurogenesis and oligodendrogenesis, and activated microglia affect oligodendrocyte progenitors at rather later stage of differentiation. We also performed the double staining of Ki67 with the respective differentiation markers (Fig. 4*B*). Although the total number of Ki67 $^+$ cells was decreased by minocycline, consistent with Figure 4*A*, the percentage of Ki67 $^+$ cells also positive for the respective differentiation markers did not change in the absence or presence of minocycline (Fig. 4*B*, left graph), suggesting that minocycline did not affect the proliferation of progenitors of the specific cell types. Typical images of the SVZ cells positive for

←

(*Figure legend continued.*) were examined by Western blotting. Minocycline significantly decreased the number of Ki67 $^+$ proliferating cells and decreased the level of nestin. The number of cells positive for Dcx was significantly reduced. Minocycline decreased the numbers of cells positive for O1 and MBP, whereas the expression level of PDGFRα tended to increase. *$p <$ 0.05, **$p <$ 0.01 (Student's t test). n = 6 mice/group. Data are mean ± SEM. ***B***, The ratio of the Ki67 $^+$ cells also positive for respective differentiation markers did not change in the absence or presence of minocycline (left graph). Typical images of the cells positive for Ki67 and Nestin, and the cells positive for Ki67 and Dcx in the control group are shown (right panels). We confirmed the same results in three independent experiments.

Ki67 and Nestin, and the cells positive for Ki67 and Dcx in the control group are shown (Fig. 4*B*, right panels).

Butovsky et al. (2006a) have reported that IGF-1 released from activated microglia promoted neurogenesis and oligodendrogenesis from adult stem/progenitor cells. We examined whether microglia in the early postnatal SVZ produce IGF-1 (Fig. 5*A*). Microglia did contain IGF-1 protein, but the percentage of CD11b$^+$ cells also positive for IGF-1$^+$ was 43.42 ± 6.72%. Furthermore, the amount of IGF-1 in the SVZ tissue lysates was not decreased by minocycline (Fig. 5*B*). These results suggest that, although a fraction of activated microglia in the early postnatal SVZ did produce IGF-1, the effects of activated microglia on neurogenesis and oligodendrogenesis obtained in our study were independent of IGF-1. Activated microglia release a number of cytokines. In some cases other than pathological conditions, cytokines also have physiological roles (Schäfers and Sorkin, 2008; Spedding and Gressens, 2008; Camacho-Arroyo et al., 2009; Miller et al., 2009; Spooren et al., 2011). We therefore investigated whether the SVZ microglia cause the increase in cytokine concentrations in the early postnatal SVZ (Fig. 5*C*). We examined the effects of minocycline on the levels of IL-1α, IL-1β, IL-2, IL-4, IL-6, IL-10, GM-CSF, IFN-γ, and TNF-α. To measure multiple cytokines in a small volume of tissue samples simultaneously, we used the BioPlex cytokine detection assay system (Bio-Rad). The levels of IL-1β, IL-6, and TNF-α were significantly decreased by the 3-day intraperitoneal administration of minocycline (Fig. 5*C*). Although the difference was not significant, the level of IFN-γ also tended to be decreased.

To examine more directly whether these cytokines affected neurogenesis and oligodendrogenesis, we performed *in vitro* experiments, coculturing neural stem cells with activated microglia. Microglia cultured independently of neurospheres on transwells were activated by LPS (10 ng/ml, 30 min) in the presence or absence of minocycline (10 μM). The microglia were carefully washed to remove residual LPS and minocycline, and then the transwell on which microglia were cultured was set onto the neurosphere cultures in prodifferentiation conditions. The activated microglia significantly increased the number of β3-tubulin$^+$ and O4$^+$ cells but had no effects on GFAP$^+$ cells in neurospheres (Fig. 6*A*,*B*). Minocycline almost completely suppressed the effects of activated microglia on the numbers of cells positive

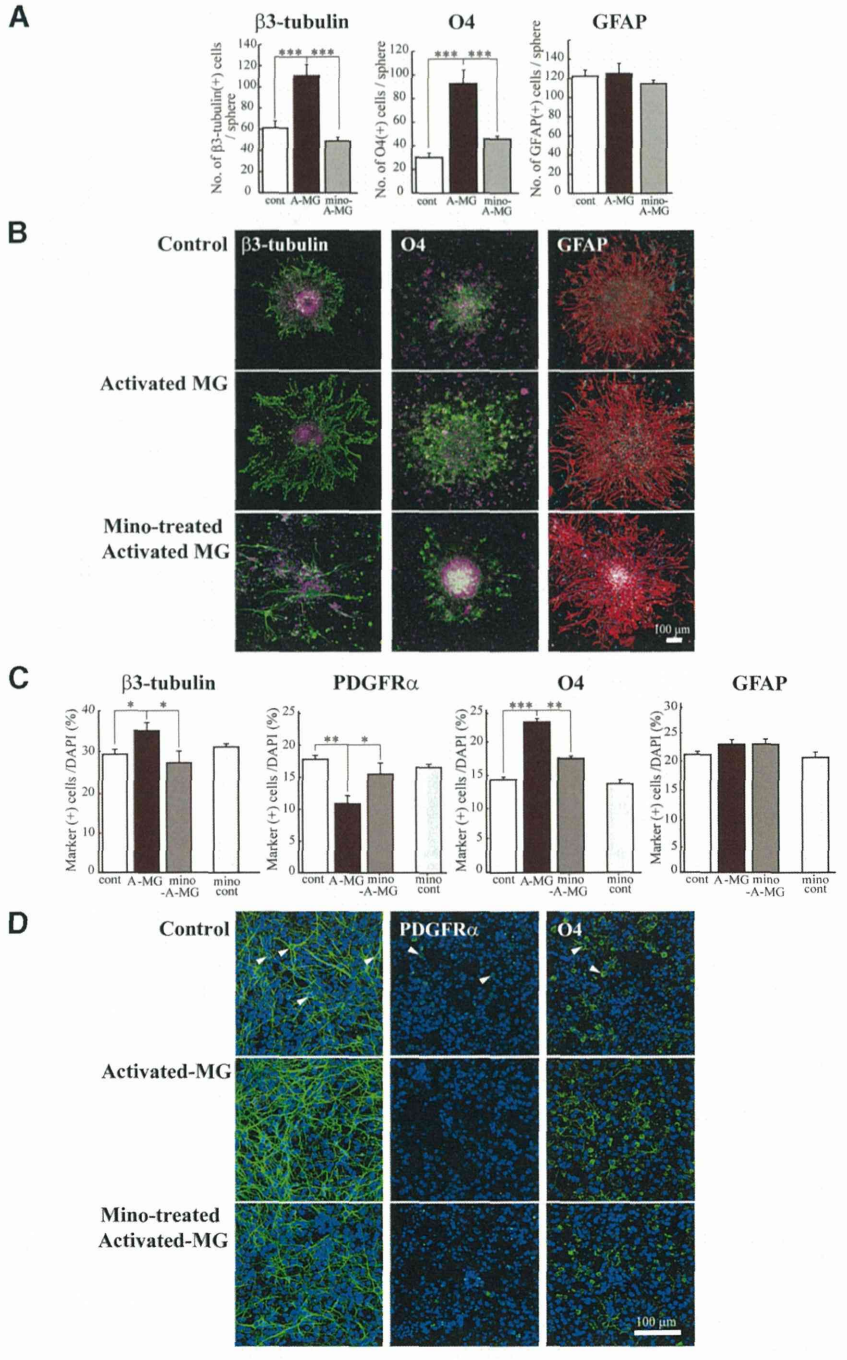

Figure 6. The reproduction of the enhancement of neurogenesis and oligodendrogenesis by activated microglia *in vitro*. Microglia cultured independently of neurosphere on transwells were activated by LPS (10 ng/ml, 30 min) in the presence or absence of minocycline (10 μM), washed carefully, and the transwells were set onto the neurospheres or dissociated cells from neurosphere in prodifferentiation conditions. After differentiation periods suitable for neurons (7 d) or oligodendrocytes (11 d), neurospheres were stained for β3-tubulin (green), PDGFRα (green), O4 (green), GFAP (red), and TOTO3 (cyan). To check the effects of minocycline alone, dissociated cells were incubated in the presence of minocycline (10 μM) for 7 d. ***A***, Quantification of the numbers of neurons, oligodendrocyte progenitors, or astrocytes differentiated from neurospheres cocultured with activated microglia in the presence or absence of minocycline. ***$p < 0.001$ (Tukey's test by ANOVA). $n = 12$ neurospheres/group. Data are mean ± SEM. ***B***, Representative immunostained images of neurospheres cocultured with activated microglia in the presence or absence of minocycline. ***C***, The effects of activated microglia on differentiation of single cells dissociated from neurospheres in the presence or absence of minocycline. The effects of minocycline alone were also shown (mino-cont in each graph). *$p < 0.05$, **$p < 0.01$, ***$p < 0.001$. (Tukey's test by ANOVA). $n = 12$ neurospheres/group. Data are mean ± SEM. ***D***, Images of cells immunostained for differentiation markers. Arrowheads indicate the representative cells positive for the differentiation markers.

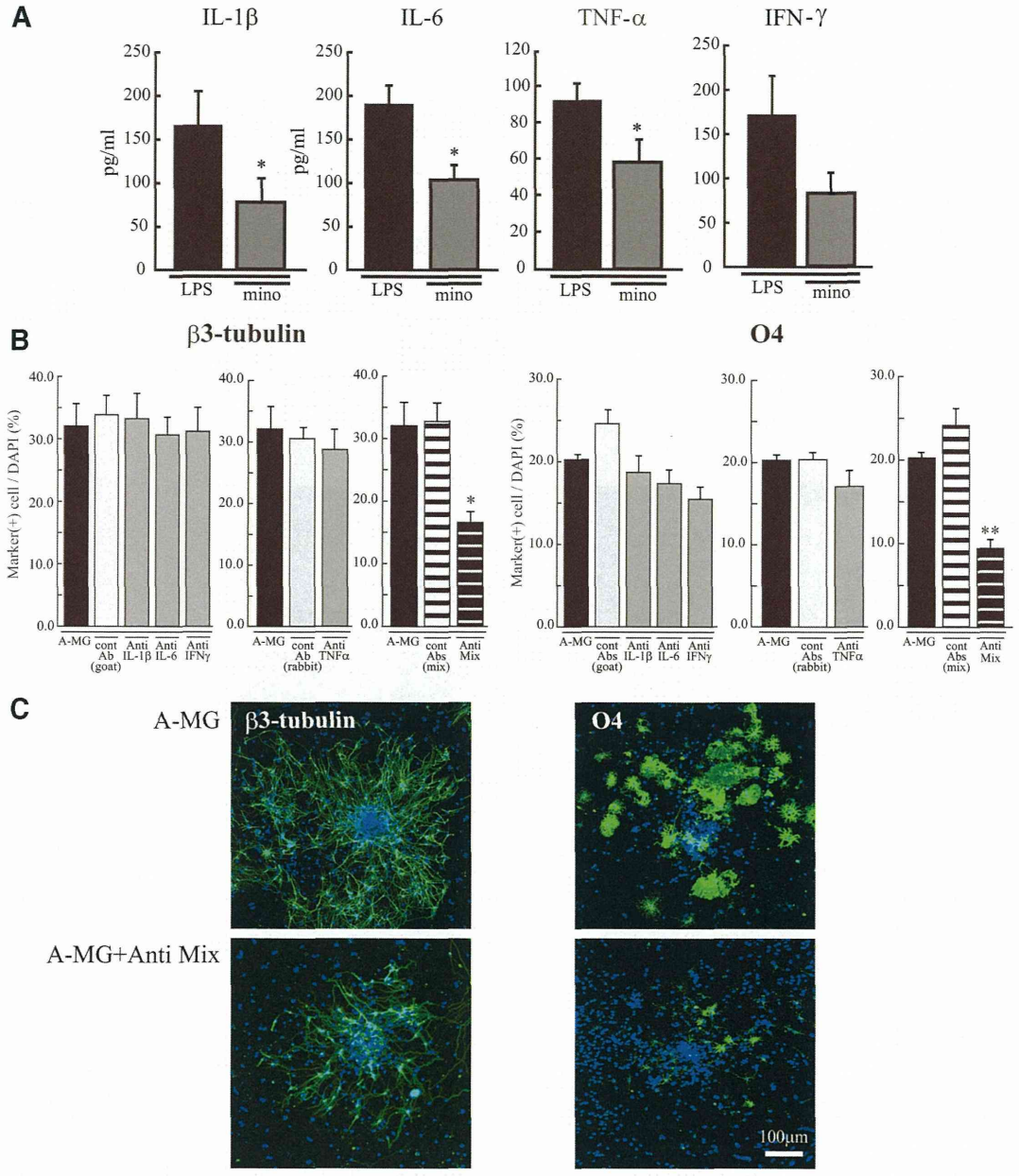

Figure 7. The *in vitro* enhancement of neurogenesis and oligodendrogenesis by activated microglia was suppressed by the mixture of function-blocking antibodies (anti-IL-1β, anti-IL-6, anti-TNF-α, and anti-IFN-γ). ***A***, The release of IL-1β, IL-6, TNF-α, or IFN-γ from activated microglia was suppressed by minocycline. Cultured microglia were activated by LPS (10 ng/ml, 30 min) in the absence and presence of minocycline (10 μM). The concentration of each cytokine in the supernatant was measured by ELISA 24 h after. *$p < 0.05$ (Student's *t* test). Data are mean ± SEM. ***B***, Effects of function-blocking antibodies to IL-1β, IL-6, TNF-α, and IFN-γ on enhanced neurogenesis and oligodendrogenesis by the activated microglia. The neurospheres were differentiated in the absence or presence of functional blocking antibodies (goat anti-rat IL-1β antibody, goat anti-rat IL-6 antibody, TNF-α antibody, or goat anti-mouse/rat IFN-γ antibody) (1 μg/ml for each) and a mixture of all of these antibodies. After a differentiation period suitable for neurons (7 d) or oligodendrocytes (11 d), neurospheres were stained for β3-tubulin (green), O4 (green), and TOTO3 (cyan). The data of single function blocking antibodies were compared with the controls, which include the same concentration of isotype-matched control IgGs (1 μg/ml for each). The data of the mixture of function blocking antibodies were compared with the controls, which include the same concentrations of isotype-matched control IgGs (i.e., 3 μg/ml of normal goat IgG control and 1 μg/ml of rabbit IgG control). *$p < 0.05$. **$p < 0.01$, versus isotype-matched control IgG group (Tukey's test by ANOVA). Data are mean ± SEM. ***C***, Representative immunostained images of neurospheres cocultured with activated microglia in the absence or presence of the mixture of the function-blocking antibodies. We confirmed the same results in three independent experiments.

for β3-tubulin or O4. We further confirmed these results using a differentiation assay with cells dissociated from neurospheres (Fig. 6*C*,*D*). With this protocol, the morphology of each cell could be discriminated more clearly. Consistent with the results described above, an increase in the numbers of cells positive for β3-tubulin and O4 was induced by activated microglia (Fig. 6*C*,*D*). Of note, PDGFRα^+ cells were decreased by activated microglia, whereas O4$^+$ cells were increased by activated microglia. Minocycline suppressed both of these effects, suggesting that activated microglia affect the later stage of oligodendrogenesis, thereby reducing the size of PDGFα^+ progenitor pool. In this experiment, we also checked the effects of minocycline alone (10 μM) on neurogenesis and oligodendrogenesis (Fig. 6*C*, "mino-cont" in each graph). Minocycline did not affect the numbers of

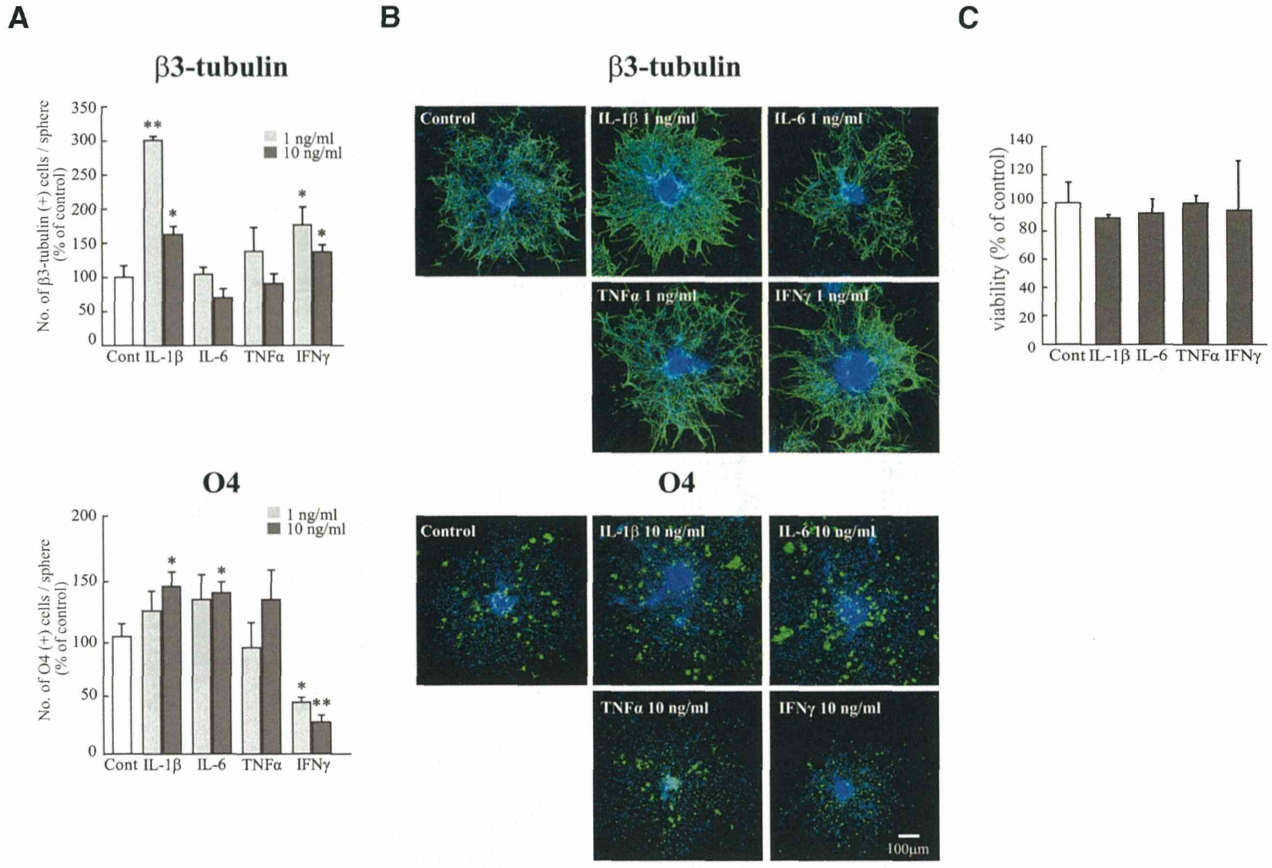

Figure 8. The effect of each cytokine on neurogenesis and oligodendrogenesis. Neurospheres were incubated for differentiation period suitable for neurons (7 d) or oligodendrocytes (11 d) in the presence of each single cytokine (rIL-1β, rIL-6, rTNF-α, or rIFN-γ) at 1–10 ng/ml. Neurospheres were stained for β3-tubulin (green), O4 (green), followed by TOTO3 (cyan). ***A***, Quantification of the effects of cytokines on neurogenesis and oligodendrogenesis. IL-1β and IFN-γ significantly enhanced neurogenesis at 1 ng/ml. IL-1β and IL-6 enhanced oligodendrogenesis at 10 ng/ml. $*p < 0.05$ versus control (Tukey's test by ANOVA). $**p < 0.01$ versus control (Tukey's test by ANOVA). $n = 8$ neurospheres/group. Data are mean ± SEM. ***B***, Representative images of neurospheres immunostained for β3-tubulin and O4 after differentiation in the presence of the cytokine. ***C***, The effect of each cytokine (10 ng/ml) on cell viability. They did not affect cell viability at 10 ng/ml. The same results were obtained in two independent experiments.

cells positive for β3-tubulin, O4, PDGFRα, or GFAP, indicating that minocycline itself had little direct effects on neurogenesis and oligodendrogenesis. Together, these results demonstrated that we could reproduce the *in vivo* data in an *in vitro* coculture experiment. We further confirmed that activated microglia enhanced neurogenesis and oligodendrogenesis, and minocycline specifically suppressed the effects of microglia. We therefore examined the effects of minocycline on the release of IL-1β, IL-6, TNF-α, and IFN-γ from activated microglia *in vitro*. In the presence of minocycline, the release of all of these cytokines was significantly suppressed (Fig. 7*A*), consistent with *in vivo* data (Fig. 5*C*). To examine the extent of the contribution of each cytokine to the enhancement of neurogenesis and oligodendrogenesis, we applied function-blocking antibodies to IL-1β, IL-6, TNF-α, and IFN-γ (1 μg/ml) to cocultures of activated microglia and neurospheres (Fig. 7*B*). The same concentration of isotype-matched control IgG (both of goat and rabbit) (1 μg/ml) did not have any effects on either neurogenesis or oligodendrogenesis. Unexpectedly, any single function-blocking antibody to IL-1β, IL-6, TNF-α, or IFN-γ did not change the effects of activated microglia on neurogenesis and oligodendrogenesis (Fig. 7*B*). We then tried a mixture of all of these function-blocking antibodies (goat anti-rat IL-1β antibody, goat anti-rat IL-6 antibody, TNF-α antibody, and goat anti-mouse/rat IFN-γ antibody, 1 μg/ml for each). When compared with the control which included the same concentrations of isotype-matched control IgGs (i.e., 3 μg/ml of normal goat IgG control and 1 μg/ml of rabbit IgG control), the effects of activated microglia were significantly suppressed by a mixture of all of these function-blocking antibodies (Fig. 7*B*, Anti Mix in the right graphs in β3-tubulin and O4, respectively). The representative images of the expression of β3-tubulin (left) or O4 (right) in neurospheres cocultured with activated microglia in the presence of the mixture of function-blocking antibodies are shown in Figure 7*C*. We also examined the direct effects of each single cytokine on neurogenesis and oligodendrogenesis separately (Fig. 8). IL-1β and IFN-γ enhanced neurogenesis at 1 ng/ml, although the effects became weaker at 10 ng/ml (Fig. 8*A*). IL-1β and IL-6 enhanced oligodendrogenesis at 10 ng/ml (Fig. 8*A*). IFN-γ suppressed oligodendrogenesis. These results suggest that IL-1β and IFN-γ are important for neurogenesis, whereas IL-1β and IL-6 are important for oligodendrogenesis, and the combinations and concentrations optimal for neurogenesis and oligodendrogenesis are different. Representative data of the neurospheres treated with the cytokines are shown in Figure 8*B*. We confirmed that each single cytokine did not affect cell viability at 10 ng/ml in our experimental protocol (Fig. 8*C*). These *in vitro* data indicate that activated microglia regulate neurogenesis and oligodendrogenesis through released cytokines, and the cyto-

kines produce their effects in a synergistic manner. It also appears that the combinations and concentrations optimal for neurogenesis and oligodendrogenesis are different.

Discussion

In the postnatal mammalian brain, neural stem cells (NSCs) are mainly localized in two areas: the forebrain SVZ (Doetsch and Scharff, 2001) and the subgranular zone of the dentate gyrus (Zerlin et al., 2004) of the hippocampus (Gould et al., 1999; Lie et al., 2004). The microenvironments that are permissive for neurogenesis and gliogenesis are composed of a variety of cell types, such as stem cells, progenitor cells, astrocyte cells, and microglial cells. Increasing evidence indicates the importance of the surrounding glial cells in neurogenesis (Doetsch et al., 1999; Temple, 2001). Goings et al. (2006) have shown that microglia in the adult SVZ are semiactivated, but microglial contribution to neurogenesis is complex. So far, the role of microglia in neurogenesis has been examined mainly in pathological conditions (Ekdahl et al., 2003; Monje et al., 2003). Activated microglia in inflammatory settings, such as intraperitoneal administration of LPS, inhibited neurogenesis (Ekdahl et al., 2003; Monje et al., 2003; Cacci et al., 2008). However, a growing number of studies have suggested that activated microglia are beneficial for neurogenesis (Aarum et al., 2003; Butovsky et al., 2005, 2006a; Walton et al., 2006; Ziv et al., 2006; Hanisch and Kettenmann, 2007; Ekdahl et al., 2009; Bachstetter et al., 2011; Ekdahl, 2012; Vukovic et al., 2012), even in pathological conditions, such as an animal model of multiple sclerosis (Butovsky et al., 2006b), ischemia (Thored et al., 2009; Deierborg et al., 2010), and epilepsy (Bonde et al., 2006). Such variability concerning the effects of microglia on neurogenesis may reflect the different polarization of microglia and/or the precise status of NSCs/neuronal progenitor cells (NPCs) (Cacci et al., 2008; Li et al., 2010; Ekdahl, 2012; Ortega et al., 2013), and crosstalk between them (Mosher et al., 2012).

Concerning the origin of microglia, various data have been reported. *In vivo* lineage tracing studies have established that microglia differentiate from primitive myeloid progenitors that arise before embryonic day 8 and are identified in the CNS parenchyma even before definitive hematopoiesis (Ginhoux et al., 2010), although it has been shown that microglia migrate from lateral ventricle into brain via SVZ in the postnatal brain (Mohri et al., 2003). Microglia in the embryonic SVZ limit the production of cortical neurons by phagocytosing neural precursor cells (Cunningham et al., 2013). Even in the adult brain, microglia appear densely populated in neurogenic niches, such as the SVZ (Mosher et al., 2012), and appear more activated in the adult SVZ than in non-neurogenic zones (Goings et al., 2006). Although these data strongly suggest that microglia play important roles in CNS development and an increasing number of studies have elucidated various roles of microglia during developmental periods (Wu et al., 1993; Pont-Lezica et al., 2011; Tremblay et al., 2011), the detailed dynamics of microglia in the SVZ from early postnatal stages to a young adult stage remain to be elucidated. Furthermore, few studies have examined the role of microglia in normal developmental processes during this period. In this study, we found that activated microglia first accumulated in the SVZ and then dispersed to white matter, where they became more ramified. In addition, the number of activated microglia was largest in the medial SVZ throughout the studied period (P30). We here elucidated that activated microglia in the early postnatal SVZ enhance neurogenesis and oligodendrogenesis through the mechanisms described below. Our present data and the previous reports concerning developmental changes in the distribution suggest that the developmental roles of microglia in the SVZ are not transient but more general throughout life.

Using a combination of *in vivo* and *in vitro* approaches, we demonstrated that these activated microglia in the early postnatal SVZ enhanced neurogenesis and oligodendrogenesis through releasing cytokines. Butovsky et al. (2006a) reported that the beneficial effects of microglia on adult neurogenesis/oligodendrogenesis was achieved by IGF-1 after IL-4 and IFN-γ release from activated microglia. In our study, although the activated microglia in the early postnatal SVZ did produce IGF-1, the effects of activated microglia on neurogenesis and oligodendrogenesis observed here were independent of IGF-1. We clarified that the SVZ microglia facilitate neurogenesis and oligodendrogenesis via production of cytokines. Interestingly, in *in vitro* coculture experiments, the enhancement of neurogenesis and oligodendrogenesis was suppressed by a mixture of function-blocking antibodies (anti-IL-1β, anti-IL-6, anti-TNF-α, anti-IFN-γ), but not by a single function-blocking antibody. These results suggest that microglial cytokines enhance neurogenesis and oligodendrogenesis in combinations. In support of this, among the cytokines we examined, only IL-1β and IFN-γ enhanced neurogenesis, whereas only IL-1β and IL-6 showed potentials of enhancing oligodendrogenesis. Previous reports have shown that NPCs express IL-1β, IL-1RI and IL-1RII, and IL-1β regulates the proliferation and differentiation of NPCs (Wang et al., 2007). It has been shown that IL-1β promotes proliferation and differentiation of oligodendrocyte progenitor cells (Vela et al., 2002). Furthermore, IL-6 and IL-6R are reported to promote neurogenesis and gliogenesis (Islam et al., 2009; Oh et al., 2010). Li et al. (2010) showed that IFN-γ stimulated neurosphere formation from embryonic brain, but the effects of IFN-γ are modified in the presence of microglia, supporting the complementary interactions between cytokines.

These proinflammatory cytokines had been thought to cause suppression of neurogenesis in pathological conditions, such as chronic LPS stimulation (Monje et al., 2003), allergic encephalomyelitis (Ben-Hur et al., 2003), and status epilepticus (Iosif et al., 2006; Koo and Duman, 2008). However, recent reports have shown that that the different polarizations of microglia are induced by different application protocols of LPS (Cacci et al., 2008), suggesting that the combination and the concentration of cytokines released by microglia change depending on the ambient conditions. Indeed, some previous reports suggest that each cytokine reveals different effects at different concentrations (Bernardino et al., 2008; Cacci et al., 2008; Das and Basu, 2008; Russo et al., 2011). Bernardino et al. (2008) have shown that TNF-α results in proliferation of neural stem cells at 1 ng/ml but caused apoptosis at 10–100 ng/ml. Microglia in the developmental brains may sense the change of environment and release a certain combination of cytokines at suitable concentrations for neurogenesis and oligodendrogenesis, whereas overactivation of microglia in pathological inflammation or nerve injury induces massive proinflammatory cytokine production, resulting in the suppression of neurogenesis. Nakanishi et al. (2007) showed that IL-6 promoted astrocytogenesis from the SVZ neurospheres. In our study, however, although activated microglia release IL-6, the effects on astrocytogenesis were not observed either *in vivo* or *in vitro*. This might be because of different medium compositions (i.e., growth factors) used for differentiation of neurosphere. Compared with the other cytokines, only IFN-γ suppressed oligodendrogenesis, suggesting that a proper concentration range of IFN-γ to enhance oligodendrogenesis might be narrower than the other cytokines.

Of interest, our results suggest that activated microglia significantly increased $O4^+$ cells while decreasing $PDGFR\alpha^+$ cells. These results suggest that activated microglia enhance oligodendrogenesis at later stages of oligodendrocyte differentiation. Recently, Miron et al. (2013) showed that a switch from M1 to M2 occurred in microglia during remyelination, and oligodendrocyte differentiation was enhanced by M2 cell releasing factors. A comprehensive analysis about the released factors from microglia, including cytokines, and the precise identification of the cell population (NSCs and/or NPCs) that are responsive to these factors will be necessary to understand fully the mechanisms underlying the effects of microglia on neurogenesis and gliogenesis.

In conclusion, we have found a population of activated microglia accumulating in the early postnatal SVZ that facilitate neurogenesis and oligodendrogenesis. A synergism among cytokines was important for the effects. To our knowledge, this is the first report to show that microglia regulate cell differentiation via releasing cytokines in early postnatal brain development.

References

Aarum J, Sandberg K, Haeberlein SL, Persson MA (2003) Migration and differentiation of neural precursor cells can be directed by microglia. Proc Natl Acad Sci U S A 100:15983–15988. CrossRef Medline

Bachstetter AD, Morganti JM, Jernberg J, Schlunk A, Mitchell SH, Brewster KW, Hudson CE, Cole MJ, Harrison JK, Bickford PC, Gemma C (2011) Fractalkine and CX 3 CR1 regulate hippocampal neurogenesis in adult and aged rats. Neurobiol Aging 32:2030–2044. CrossRef Medline

Ben-Hur T, Ben-Menachem O, Furer V, Einstein O, Mizrachi-Kol R, Grigoriadis N (2003) Effects of proinflammatory cytokines on the growth, fate, and motility of multipotential neural precursor cells. Mol Cell Neurosci 24:623–631. CrossRef Medline

Bernardino L, Agasse F, Silva B, Ferreira R, Grade S, Malva JO (2008) Tumor necrosis factor-alpha modulates survival, proliferation, and neuronal differentiation in neonatal subventricular zone cell cultures. Stem Cells 26:2361–2371. CrossRef Medline

Bonde S, Ekdahl CT, Lindvall O (2006) Long-term neuronal replacement in adult rat hippocampus after status epilepticus despite chronic inflammation. Eur J Neurosci 23:965–974. CrossRef Medline

Butovsky O, Talpalar AE, Ben-Yaakov K, Schwartz M (2005) Activation of microglia by aggregated beta-amyloid or lipopolysaccharide impairs MHC-II expression and renders them cytotoxic whereas IFN-gamma and IL-4 render them protective. Mol Cell Neurosci 29:381–393. CrossRef Medline

Butovsky O, Ziv Y, Schwartz A, Landa G, Talpalar AE, Pluchino S, Martino G, Schwartz M (2006a) Microglia activated by IL-4 or IFN-gamma differentially induce neurogenesis and oligodendrogenesis from adult stem/progenitor cells. Mol Cell Neurosci 31:149–160. CrossRef Medline

Butovsky O, Landa G, Kunis G, Ziv Y, Avidan H, Greenberg N, Schwartz A, Smirnov I, Pollack A, Jung S, Schwartz M (2006b) Induction and blockage of oligodendrogenesis by differently activated microglia in an animal model of multiple sclerosis. J Clin Invest 116:905–915. CrossRef Medline

Cacci E, Ajmone-Cat MA, Anelli T, Biagioni S, Minghetti L (2008) In vitro neuronal and glial differentiation from embryonic or adult neural precursor cells are differently affected by chronic or acute activation of microglia. Glia 56:412–425. CrossRef Medline

Camacho-Arroyo I, López-Griego L, Morales-Montor J (2009) The role of cytokines in the regulation of neurotransmission. Neuroimmunomodulation 16:1–12. CrossRef Medline

Cunningham CL, Martínez-Cerdeño V, Noctor SC (2013) Microglia regulate the number of neural precursor cells in the developing cerebral cortex. J Neurosci 33:4216–4233. CrossRef Medline

Das S, Basu A (2008) Inflammation: a new candidate in modulating adult neurogenesis. J Neurosci Res 86:1199–1208. CrossRef Medline

Deierborg T, Roybon L, Inacio AR, Pesic J, Brundin P (2010) Brain injury activates microglia that induce neural stem cell proliferation ex vivo and promote differentiation of neurosphere-derived cells into neurons and oligodendrocytes. Neuroscience 171:1386–1396. CrossRef Medline

Doetsch F, Scharff C (2001) Challenges for brain repair: insights from adult neurogenesis in birds and mammals. Brain Behav Evol 58:306–322. CrossRef Medline

Doetsch F, García-Verdugo JM, Alvarez-Buylla A (1999) Regeneration of a germinal layer in the adult mammalian brain. Proc Natl Acad Sci U S A 96:11619–11624. CrossRef Medline

Ekdahl CT (2012) Microglial activation- tuning and pruning adult neurogenesis. Front Pharmacol 3:41. CrossRef Medline

Ekdahl CT, Claasen JH, Bonde S, Kokaia Z, Lindvall O (2003) Inflammation is detrimental for neurogenesis in adult brain. Proc Natl Acad Sci U S A 100:13632–13637. CrossRef Medline

Ekdahl CT, Kokaia Z, Lindvall O (2009) Brain inflammation and adult neurogenesis: the dual role of microglia. Neuroscience 158:1021–1029. CrossRef Medline

Ginhoux F, Greter M, Leboeuf M, Nandi S, See P, Gokhan S, Mehler MF, Conway SJ, Ng LG, Stanley ER, Samokhvalov IM, Merad M (2010) Fate mapping analysis reveals that adult microglia derive from primitive macrophages. Science 330:841–845. CrossRef Medline

Goings GE, Kozlowski DA, Szele FG (2006) Differential activation of microglia in neurogenic versus non-neurogenic regions of the forebrain. Glia 54:329–342. CrossRef Medline

Gould E, Reeves AJ, Graziano MS, Gross CG (1999) Neurogenesis in the neocortex of adult primates. Science 286:548–552. CrossRef Medline

Hamanoue M, Matsuzaki Y, Sato K, Okano HJ, Shibata S, Sato I, Suzuki S, Ogawara M, Takamatsu K, Okano H (2009) Cell surface N-glycans mediated isolation of mouse neural stem cells. J Neurochem 110:1575–1584. CrossRef Medline

Hanisch UK, Kettenmann H (2007) Microglia: active sensor and versatile effector cells in the normal and pathologic brain. Nat Neurosci 10:1387–1394. CrossRef Medline

Hirasawa T, Ohsawa K, Imai Y, Ondo Y, Akazawa C, Uchino S, Kohsaka S (2005) Visualization of microglia in living tissues using Iba1-EGFP transgenic mice. J Neurosci Res 81:357–362. CrossRef Medline

Ignácio AR, Müller YM, Carvalho MS, Nazari EM (2005) Distribution of microglial cells in the cerebral hemispheres of embryonic and neonatal chicks. Braz J Med Biol Res 38:1615–1621. Medline

Inoue K (2008) Purinergic systems in microglia. Cell Mol Life Sci 65:3074–3080. CrossRef Medline

Iosif RE, Ekdahl CT, Ahlenius H, Pronk CJ, Bonde S, Kokaia Z, Jacobsen SE, Lindvall O (2006) Tumor necrosis factor receptor 1 is a negative regulator of progenitor proliferation in adult hippocampal neurogenesis. J Neurosci 26:9703–9712. CrossRef Medline

Islam O, Gong X, Rose-John S, Heese K (2009) Interleukin-6 and neural stem cells: more than gliogenesis. Mol Biol Cell 20:188–199. CrossRef Medline

Kettenmann H, Hanisch UK, Noda M, Verkhratsky A (2011) Physiology of microglia. Physiol Rev 91:461–553. CrossRef Medline

Koo JW, Duman RS (2008) IL-1beta is an essential mediator of the antineurogenic and anhedonic effects of stress. Proc Natl Acad Sci U S A 105:751–756. CrossRef Medline

Li L, Walker TL, Zhang Y, Mackay EW, Bartlett PF (2010) Endogenous interferon gamma directly regulates neural precursors in the non-inflammatory brain. J Neurosci 30:9038–9050. CrossRef Medline

Lie DC, Song H, Colamarino SA, Ming GL, Gage FH (2004) Neurogenesis in the adult brain: new strategies for central nervous system diseases. Annu Rev Pharmacol Toxicol 44:399–421. CrossRef Medline

Marshall GP 2nd, Demir M, Steindler DA, Laywell ED (2008) Subventricular zone microglia possess a unique capacity for massive in vitro expansion. Glia 56:1799–1808. CrossRef Medline

Miller RJ, Jung H, Bhangoo SK, White FA (2009) Cytokine and chemokine regulation of sensory neuron function. Handb Exp Pharmacol 194:417–449. CrossRef Medline

Miron VE, Boyd A, Zhao JW, Yuen TJ, Ruckh JM, Shadrach JL, van Wijngaarden P, Wagers AJ, Williams A, Franklin RJ, ffrench-Constant C (2013) M2 microglia and macrophages drive oligodendrocyte differentiation during CNS remyelination. Nat Neurosci 16:1211–1218. CrossRef Medline

Mohri I, Eguchi N, Suzuki K, Urade Y, Taniike M (2003) Hematopoietic prostaglandin D synthase is expressed in microglia in the developing postnatal mouse brain. Glia 42:263–274. CrossRef Medline

Monje ML, Toda H, Palmer TD (2003) Inflammatory blockade restores adult hippocampal neurogenesis. Science 302:1760–1765. CrossRef Medline

Monji A, Kato T, Kanba S (2009) Cytokines and schizophrenia: microglia

hypothesis of schizophrenia. Psychiatry Clin Neurosci 63:257–265. CrossRef Medline

Mosher KI, Andres RH, Fukuhara T, Bieri G, Hasegawa-Moriyama M, He Y, Guzman R, Wyss-Coray T (2012) Neural progenitor cells regulate microglia functions and activity. Nat Neurosci 15:1485–1487. CrossRef Medline

Nakajima K, Kohsaka S (2001) Microglia: activation and their significance in the central nervous system. J Biochem 130:169–175. CrossRef Medline

Nakajima K, Tsuzaki N, Shimojo M, Hamanoue M, Kohsaka S (1992) Microglia isolated from rat brain secrete a urokinase-type plasminogen activator. Brain Res 577:285–292. CrossRef Medline

Nakanishi M, Niidome T, Matsuda S, Akaike A, Kihara T, Sugimoto H (2007) Microglia-derived interleukin-6 and leukaemia inhibitory factor promote astrocytic differentiation of neural stem/progenitor cells. Eur J Neurosci 25:649–658. CrossRef Medline

Nishiyama A, Komitova M, Suzuki R, Zhu X (2009) Polydendrocytes (NG2 cells): multifunctional cells with lineage plasticity. Nat Rev Neurosci 10: 9–22. CrossRef Medline

Oh J, McCloskey MA, Blong CC, Bendickson L, Nilsen-Hamilton M, Sakaguchi DS (2010) Astrocyte-derived interleukin-6 promotes specific neuronal differentiation of neural progenitor cells from adult hippocampus. J Neurosci Res 88:2798–2809. CrossRef Medline

Ortega F, Gascón S, Masserdotti G, Deshpande A, Simon C, Fischer J, Dimou L, Chichung Lie D, Schroeder T, Berninger B (2013) Oligodendrogliogenic and neurogenic adult subependymal zone neural stem cells constitute distinct lineages and exhibit differential responsiveness to Wnt signalling. Nat Cell Biol 15:602–613. CrossRef Medline

Pont-Lezica L, Béchade C, Belarif-Cantaut Y, Pascual O, Bessis A (2011) Physiological roles of microglia during development. J Neurochem 119: 901–908. CrossRef Medline

Reynolds BA, Tetzlaff W, Weiss S (1992) A multipotent EGF-responsive striatal embryonic progenitor cell produces neurons and astrocytes. J Neurosci 12:4565–4574. Medline

Russo I, Barlati S, Bosetti F (2011) Effects of neuroinflammation on the regenerative capacity of brain stem cells. J Neurochem 116:947–956. CrossRef Medline

Schäfers M, Sorkin L (2008) Effect of cytokines on neuronal excitability. Neurosci Lett 437:188–193. CrossRef Medline

Spedding M, Gressens P (2008) Neurotrophins and cytokines in neuronal plasticity. Novartis Found Symp 289:222–233; discussion 233–240. Medline

Spooren A, Kolmus K, Laureys G, Clinckers R, De Keyser J, Haegeman G, Gerlo S (2011) Interleukin-6, a mental cytokine. Brain Res Rev 67:157–183. CrossRef Medline

Suzuki SO, Goldman JE (2003) Multiple cell populations in the early postnatal subventricular zone take distinct migratory pathways: a dynamic study of glial and neuronal progenitor migration. J Neurosci 23:4240–4250. Medline

Temple S (2001) The development of neural stem cells. Nature 414:112–117. CrossRef Medline

Thored P, Heldmann U, Gomes-Leal W, Gisler R, Darsalia V, Taneera J, Nygren JM, Jacobsen SE, Ekdahl CT, Kokaia Z, Lindvall O (2009) Long-term accumulation of microglia with proneurogenic phenotype concomitant with persistent neurogenesis in adult subventricular zone after stroke. Glia 57:835–849. CrossRef Medline

Tikka T, Fiebich BL, Goldsteins G, Keinanen R, Koistinaho J (2001) Minocycline, a tetracycline derivative, is neuroprotective against excitotoxicity by inhibiting activation and proliferation of microglia. J Neurosci 21: 2580–2588. Medline

Tremblay MÈ, Stevens B, Sierra A, Wake H, Bessis A, Nimmerjahn A (2011) The role of microglia in the healthy brain. J Neurosci 31:16064–16069. CrossRef Medline

Vela JM, Molina-Holgado E, Arévalo-Martín A, Almazán G, Guaza C (2002) Interleukin-1 regulates proliferation and differentiation of oligodendrocyte progenitor cells. Mol Cell Neurosci 20:489–502. CrossRef Medline

Vukovic J, Colditz MJ, Blackmore DG, Ruitenberg MJ, Bartlett PF (2012) Microglia modulate hippocampal neural precursor activity in response to exercise and aging. J Neurosci 32:6435–6443. CrossRef Medline

Wagner JP, Black IB, DiCicco-Bloom E (1999) Stimulation of neonatal and adult brain neurogenesis by subcutaneous injection of basic fibroblast growth factor. J Neurosci 19:6006–6016. Medline

Walton NM, Sutter BM, Laywell ED, Levkoff LH, Kearns SM, Marshall GP 2nd, Scheffler B, Steindler DA (2006) Microglia instruct subventricular zone neurogenesis. Glia 54:815–825. CrossRef Medline

Wang X, Fu S, Wang Y, Yu P, Hu J, Gu W, Xu XM, Lu P (2007) Interleukin-1beta mediates proliferation and differentiation of multipotent neural precursor cells through the activation of SAPK/JNK pathway. Mol Cell Neurosci 36:343–354. CrossRef Medline

Wu CH, Wen CY, Shieh JY, Ling EA (1993) A quantitative study of the differentiation of microglial cells in the developing cerebral cortex in rats. J Anat 182:403–413. Medline

Xu J, Ling EA (1994) Studies of the distribution and functional roles of transitory amoeboid microglial cells in developing rat brain using exogenous horseradish peroxidase as a marker. J Hirnforsch 35:103–111. Medline

Zerlin M, Milosevic A, Goldman JE (2004) Glial progenitors of the neonatal subventricular zone differentiate asynchronously, leading to spatial dispersion of glial clones and to the persistence of immature glia in the adult mammalian CNS. Dev Biol 270:200–213. CrossRef Medline

Zhao C, Ling Z, Newman MB, Bhatia A, Carvey PM (2007) TNF-alpha knockout and minocycline treatment attenuates blood–brain barrier leakage in MPTP-treated mice. Neurobiol Dis 26:36–46. CrossRef Medline

Ziv Y, Ron N, Butovsky O, Landa G, Sudai E, Greenberg N, Cohen H, Kipnis J, Schwartz M (2006) Immune cells contribute to the maintenance of neurogenesis and spatial learning abilities in adulthood. Nat Neurosci 9:268–275. CrossRef Medline

Fundamental Toxicological Sciences (Fund. Toxicol. Sci.)
Vol.1, No.3, 87-94, 2014

Original Article

Residual metals in carbon nanotubes suppress the proliferation of neural stem cells

Yukari Shigemoto-Mogami[1], Koki Fujimori[1,2], Yoshiaki Ikarashi[3], Akihiko Hirose[4], Yuko Sekino[1] and Kaoru Sato[1]

[1]*Laboratory of Neuropharmacology, Division of Pharmacology, National Institute of Health Sciences, 1-18-1 Kamiyoga, Setagaya-ku, Tokyo 158-8501, Japan*
[2]*Division of Basic Biological Science, Faculty of Pharmacy, Keio University, 1-5-30 Shiba-koen, Minato-ku, Tokyo 105-8512, Japan*
[3]*Division of Environmental Chemistry, National Institute of Health Sciences, 1-18-1 Kamiyoga, Setagaya-ku, Tokyo 158-8501, Japan*
[4]*Division of Risk Assessment, National Institute of Health Sciences, 1-18-1 Kamiyoga, Setagaya-ku, Tokyo 158-8501, Japan*

(Received October 17, 2014; Accepted October 20, 2014)

ABSTRACT — Carbon nanotubes (CNTs) are used in many fields; however, little is known about the effects of CNTs on the central nervous system (CNS). In this study, we found that extracts of sonicated CNTs suppressed the proliferation of neural stem cells (NSCs). Single-walled CNTs (SWCNTs) and multiple-walled CNTs (MWCNTs) were suspended in PBS (1 mg/mL) and sonicated for 5 hr using a water bath sonicator. Supernatants from both types of CNTs suppressed NSC proliferation. The effects weakened in a dilution-ratio-dependent manner and strengthened in a sonication time-dependent manner. Metal concentrations extracted from SCNTs and MCNTs after 5-hr of sonication were determined using inductively coupled plasma mass spectrometry. Mn, Rb, Cs, Tl, and Fe were detected in the SWCNT supernatant, and Mn, Cs, W, and Tl were detected in the MWCNT supernatant. The concentration of Mn, Rb, and Fe eluted from the SWCNTs and Rb eluted from MWCNTs following sonication were sufficient to suppress NSC proliferation alone. N-acetyl cysteine (NAC) and ascorbic acid (AA) reversed the effects of Mn and Fe and restored NSC proliferation. The effects of Rb and Tl were not affected by the antioxidants. Both antioxidants largely restored the suppression of NSC proliferation induced by the SWCNT and MWCNT supernatants. These results suggest that metals extracted from CNTs via a strong vibration energy can suppress NSC proliferation through ROS production by the extracted metals.

Key words: Carbon nanotube, Neural stem cell, Metals, Proliferation

INTRODUCTION

CNTs are fiber-shaped nanomaterials that consist of graphite hexagonal-mesh planes (graphene sheet) in a single-layer (single-walled carbon nanotubes (SWCNTs)) or in multiple layers with nest accumulation (multi-walled carbon nanotubes (MWCNTs)). The structure of SWCNTs is a honeycomb carbon lattice rolled into a cylinder, and the basic morphology consists of a sheet of tangled SWCNT (with a diameter of approximately 2 nm) bundles with diameters tens of nanometers in length. The structure of MWCNTs consists of honeycomb carbon lattices rolled into a multi-layer tubular shape, and the basic morphology is composed of particles of tangled MWCNTs with a diameter of approximately 30 nm. CNTs are used in many fields, including energy, healthcare, environment, materials, and electronics. However, adverse effects of CNTs on human health are poorly understood. Exposure to asbestos is known to cause asbestosis, bronchogenic carcinoma, mesothelioma, pleural fibrosis and pleural plaques, indicating that both the lungs and the pleura are targets of asbestos (Donaldson *et al.*, 2013). CNTs also exist as fibers or compact particles; thus, most studies concerning the adverse effects of CNTs have focused on lung toxicity (Jaurand *et al.*, 2009; Pacurari *et al.*, 2010) based on the fiber pathogenicity paradigm developed in the 1970-80s.

Correspondence: Kaoru Sato (E-mail: kasato@nihs.go.jp)

However, recent reports showed that nano-particles can cross the blood–brain barrier (BBB) and enter the brain (Sharma and Sharma, 2007). Furthermore, it has been suggested that the olfactory nerve pathway is a portal of entry into the CNS (Henriksson and Tjalve, 2000; Persson *et al.*, 2003; Mistry *et al.*, 2009; Balasubramanian *et al.*, 2013). Recent reports showed that MWCNTs are toxic to neural cells (Belyanskaya *et al.*, 2009; Xu *et al.*, 2009; Gavello *et al.*, 2012). Here, we investigated the effects of CNTs on the self-renewal of neural stem cells (NSCs). The mammalian CNS comprises various cell types, including neurons, astrocytes, and oligodendrocytes, and these cells differentiate from NSCs at specific brain developmental stages. Sufficient proliferation of NSCs before differentiation is essential to supply the neurons and glia required for brain function (Caviness *et al.*, 1995; Kriegstein and Alvarez-Buylla, 2009). In addition, NSCs are maintained in the subventricular zone and the hippocampal subgranular zone in the adult brain. Adult neurogenesis from these NSCs plays a key role in higher-order brain functions, such as cognition, learning and memory (Couillard-Despres *et al.*, 2011; Eisch and Petrik, 2012; Rolando and Taylor, 2014). Thus, the effects of CNTs on the proliferation of NSCs need to be determined for both of brain development and brain function. Here, we report that sonicated extracts of CNTs suppressed the proliferation of NSCs. We also determined that these effects were mediated through ROS produced by residual metals in the CNTs.

MATERIALS AND METHODS

Materials

CNTs (SWCNT: purity > 95%; Lot No.: SW1859; MWCNT: purity: > 98%; Lot No.: 04-12/10#1-(4)) were supplied by Nikkiso Co., Ltd. (Shizuoka, Japan). Both test materials were not coated or modified. The detailed physiochemical properties of Nikkiso CNTs have been previously reported (Ema *et al.*, 2011; Matsumoto *et al.*, 2012). Epidermal growth factor (EGF), $MnCl_2$, RbCl, $TlCl_3$, $FeCl_2$, $FeCl_3$, and NAC were purchased from Sigma (St. Louis, Mo, USA). Fibroblast growth factor 2 (FGF2) was purchased from PeproTech (Rocky Hill, NJ, USA). AA was purchased from WAKO (Osaka, Japan). The BrdU cell proliferation assay kit was purchased from Merck (Darmstadt, Germany). B27 supplement, TrypLE Select, FBS, and DMEM were purchased from Life Technologies (Grand Island, NY, USA).

Preparation of supernatants of sonicated CNT solutions

SWCNTs and MWCNTs were suspended in PBS (1 mg/mL) and sonicated for 10 min or 5 hr using a water bath-sonicator (Hitachi-Kokusai Electric Inc., Tokyo, Japan) at a frequency of 36 kHz and a watt density of 65 W/264 cm^2. The supernatants of sonicated CNT suspensions were diluted with culture medium 10- to 1,000-fold.

Rat neural stem cell (NSC) culture

Rat NSCs were cultured as previously described (Reynolds *et al.*, 1992; Hamanoue *et al.*, 2009) with slight modifications. Briefly, the telencephalons were dissected from embryonic day 16 (E16) rats of either sex in ice-cold DMEM/F12. The tissue was then minced and dispersed into single cells by pipetting. Cells were then cultured in DMEM/F12 containing B27 supplement (1/200), 20 ng/mL fibroblast growth factor 2 (FGF2) and 20 ng/mL epidermal growth factor (EGF) for 7 days. The primary neurospheres were incubated with TrypLE Select for 15 min and dissociated by pipetting. Single cells were seeded in 96-well plates for the proliferation assay.

Measurement of metal concentrations

CNTs were suspended in PBS (1 mg/mL) and sonicated for 5 hr using a water bath sonicator. The metal concentrations in the CNT supernatants were quantified using an inductively coupled plasma mass spectrometer (ICP-MS) (Agilent 7500ce ICP-MS, Agilent Technologies, Santa Clara, CA, USA) fitted with a collision/reaction cell in helium mode. We first detected metals at concentrations exceeding the detection limits using a semi-quantitative analysis. Next, we determined the concentration of the detected metals (i.e., Mn, Fe, Rb, Cs, W, and TI) using a full quantitative analysis with calibration curves.

Treatment of NSCs with the supernatants of sonicated CNT suspensions, metals, and antioxidants

NSCs were treated with the supernatants of sonicated CNT suspensions, $MnCl_2$ (1-100 ppb), RbCl (1-100 ppb), $TlCl_3$ (0.1-10 ppb), $FeCl_2$ (100-10,000 ppb) or $FeCl_3$ (100-10,000 ppb) with or without 10 μM N-acetyl cysteine (NAC) or 10 μM ascorbic acid (AA) for 24 hr.

NSC proliferation assay

We quantified NSC proliferation according the instructions from the BrdU cell proliferation assay kit (Calbiochem, Hayward, CA, USA). The primary neurospheres were dissociated into single cells and seeded in 96-well plates at a density of 2 x 10^4 cells/

well. BrdU was added to the medium during the treatment of NSCs. After incubation, the cells were fixed, and BrdU-immuno-labeling was performed. The fluorescence intensities were used as a marker of proliferation. The fluorescence was measured at an excitation wavelength of 320 nm and emission wavelength of 460 nm with a fluorescence microplate reader (Spectra Max Microplate reader, Molecular Devices, Sunnyvale, CA, USA).

Data analysis and statistics

All data are shown as the mean ± S.E.M. The statistical analysis was performed using Student's *t*-test or an ANOVA followed by a Tukey's test. Differences were considered to be significant at $p < 0.05$.

RESULTS

SWCNTs and MWCNTs were suspended in PBS (1 mg/mL) and sonicated for 5 hr using a water bath sonicator. The supernatants of the sonicated CNT suspensions were collected and diluted with culture medium 10- to 1,000-fold. We found that a 24-hr treatment with supernatants of SWCNT and MWCNT suppressed NSC proliferation in a dilution ratio-dependent manner (Fig. 1). The suppression of proliferation was stronger with the SWCNT supernatant when compared with the MWCNT supernatant. The effects of sonication time were also assessed. The suppressive effects of both supernatants disappeared when the sonication time was changed from 5 hr to 10 min (Fig. 2). These results suggest that the suppression of NSC proliferation is due to factors released from CNTs in a sonication time-dependent manner.

CNTs are manufactured using metallic catalysts (Ding *et al.*, 2008; Yazyev and Pasquarello, 2008; Banhart, 2009; Tyagi *et al.*, 2011). Thus, we speculated that residual metals extracted from CNTs during the 5-hr sonication may be responsible for the suppression of NSC proliferation. We therefore quantified the metal contents in the CNT supernatants. The metals in the SWCNT and MWCNT supernatants were first analyzed using ICP-MS in a semi-quantitative mode. Next, the concentrations of metals were determined using calibration curves (Table 1). We found that a 5-hr sonication induced the extraction of multiple metals from the CNTs. Mn, Rb, Cs, Tl, and Fe were detected in the SWCNT supernatant, whereas Mn, Cs, W, and Tl were detected in the MWCNT supernatant. Among these metals, the concentration of Fe in SWCNT supernatant was remarkably high (from N.D. to 7,110 ppb). The concentrations of these metals in PBS were largely negligible and did not change after a 5-hr sonication.

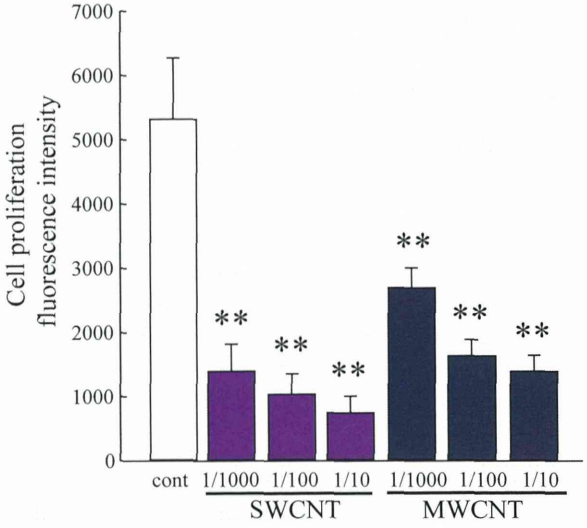

Fig. 1. Effects of the supernatants of sonicated CNT suspensions on the proliferation of rat NSCs. The supernatants of SWCNTs and MWCNTs suppressed NSC proliferation in a dilution ratio-dependent manner. *: $p < 0.05$, **: $p < 0.01$ vs. control group ($N = 6$), ANOVA followed by a Tukey's test.

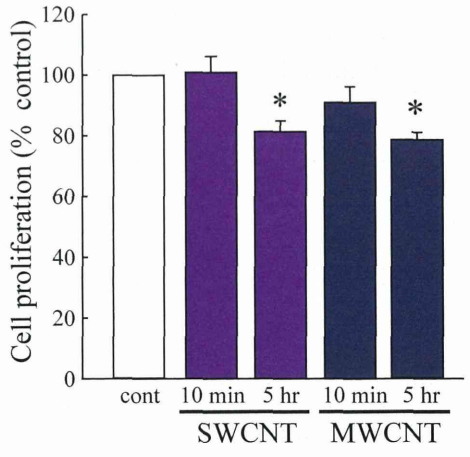

Fig. 2. Sonication time-dependence of CNT supernatant effects. The effects of SWCNT and MWCNT supernatants disappeared with a sonication time of 10 min. However, a 5-hr sonication time produced a significant suppression of NSC proliferation. *: $p < 0.05$ vs. control group ($N = 6$), ANOVA followed by a Tukey's test.

Next, we examined the direct effects of the metals at concentration ranges detected in the supernatants. Fig. 3 shows the metals that had a suppressive effect on NSC

Table 1. Metals eluted from CNTs by sonication for 5 hr.

	Concentrations of metals (ppb) 1 ppb = 10^{-8}%					
	PBS	PBS	SWCNT	SWCNT	MWCNT	MWCNT
sonication	-	+	-	+	-	+
Mn	nd	nd	0.33	16.04	nd	0.26
Rb	3.97	3.84	6.88	13.33	4.06	4.61
Cs	nd	nd	0.1	0.32	nd	0.59
W	nd	0.05	nd	0.08	nd	0.4
Tl	md	nd	0.05	0.17	nd	0.37
Fe	nd	nd	nd	7110	nd	nd

The metal concentrations in the supernatant of SWCNT and MWCNT were quantified using ICP-MS in a semi-quantitative mode followed by a full quantitative mode. Mn, Rb, Cs, W, Tl, and Fe were detected in the SWCNT supernatant. Mn, Rb, Cs, W, Tl, and Fe were detected in the MWCNT supernatant. The concentration of Fe in the SWCNT supernatant was remarkably high (7,110 ppb).

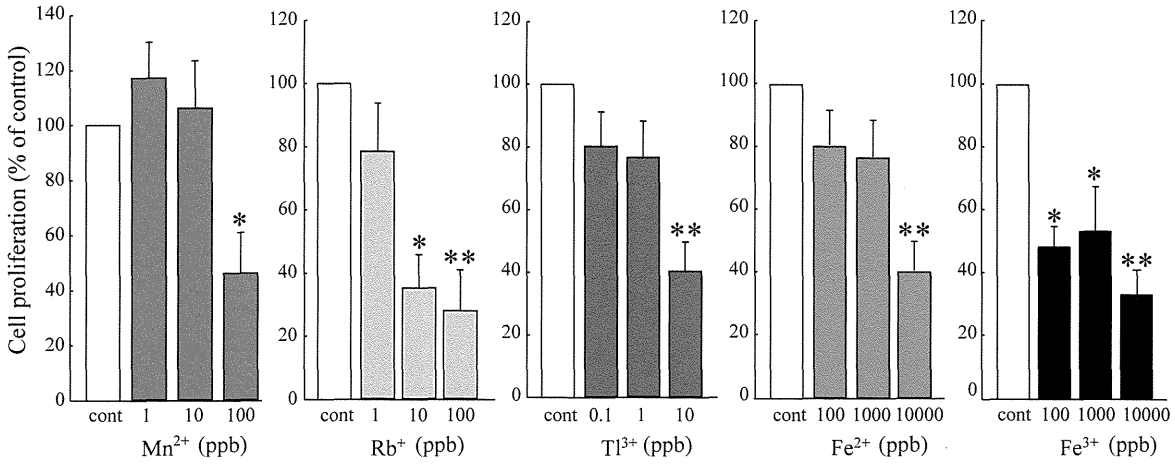

Fig. 3. The direct effect of metals in CNT supernatants. Mn^{2+}, Rb^{+}, Tl^{3+}, Fe^{2+}, and Fe^{3+} suppressed NSC proliferation in a concentration-dependent manner. *: $p < 0.05$, **: $p < 0.01$ vs. control group (N = 12), ANOVA followed by a Tukey's test.

proliferation (Fig. 3). Mn^{2+}, Rb^{+}, Tl^{3+}, Fe^{2+}, and Fe^{3+} suppressed the proliferation of NSCs in a concentration-dependent manner. These results indicate that Mn, Rb, and Fe were present in the SWCNT supernatant at a concentration high enough to suppress NSC proliferation. This effect was induced by the Rb in the MWCNT supernatant. Some metals are known to produce reactive oxygen species (Ding *et al.*, 2008) that can result in oxidative stress on lipids, DNA and proteins (Henriksson and Tjalve, 2000; Choi *et al.*, 2007; Alekseenko *et al.*, 2008; Kim *et al.*, 2011; Latronico *et al.*, 2013; Roth and Eichhorn, 2013; Sripetchwandee *et al.*, 2013). Thus, we examined the involvement of ROS in the suppression of NSC proliferation. N-acetyl cysteine (NAC) (10 μM) and ascorbic acid (AA) (10 μM) are typical antioxidants that can significantly restore the suppression of the NSC proliferation caused by Mn^{2+}, Fe^{2+}, and Fe^{3+} (Fig. 4A). The effect of Rb and Tl were not affected by NAC or AA (data not shown). These results suggest that ROS is involved in the suppressive effects produced by Mn and Fe. We also examined whether ROS played a role in the suppression of NSC proliferation by the CNT supernatants (Fig. 4B). Both NAC and AA markedly restored the decrease in NSC proliferation caused by the SWCNT and MWCNT supernatants. We confirmed that both of these antioxidants alone did not affect NSC proliferation (data not shown). Taken together, these results suggest that the suppressive effects of the sonicated extract of CNTs were mainly caused by

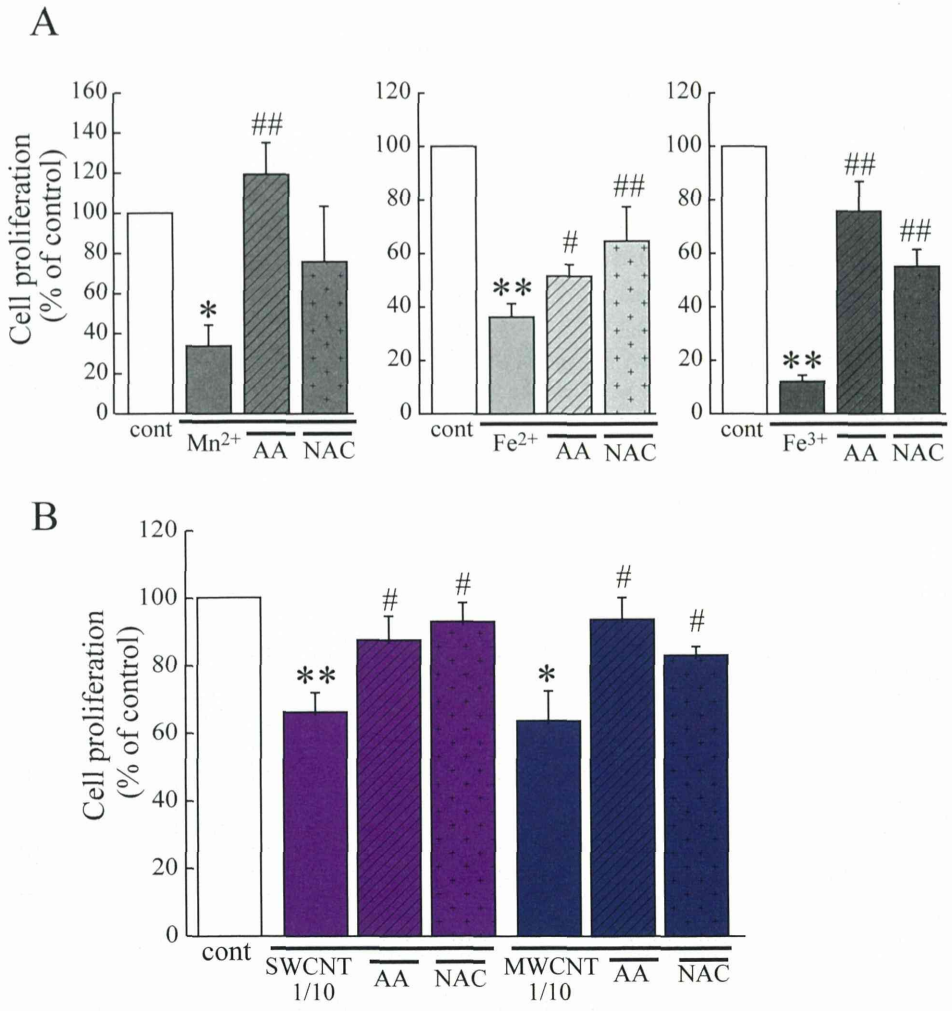

Fig. 4. Antioxidants attenuated the reduction in NSC proliferation caused by metals and CNT supernatants. The suppression of the NSC proliferation caused by Mn^{2+}, Fe^{2+}, Fe^{3+} (A) and the supernatants of CNTs (B) was significantly restored by NAC (10 μM) and AA (10 μM). *: $p < 0.05$,**: $p < 0.01$ vs. control group, #: $p < 0.05$, ##: $p < 0.01$ vs. metal or CNT-supernatant-treated groups (N = 7), ANOVA followed by a Tukey's test.

ROS produced by residual metals.

DISCUSSION

We found that the supernatants of sonicated CNT suspensions suppress NSC proliferation. We also determined that these effects were largely mediated by ROS production from residual metals. To demonstrate the involvement of ROS, we used the two antioxidants NAC and AA. NAC exerts its protective by increasing glutathione levels (Yim *et al.*, 1994; Arfsten *et al.*, 2007; Li *et al.*, 2009), directly scavenging ROS, and activating ERK1/2 (Zhang *et al.*, 2011). AA is a powerful water-soluble antioxidant that acts by scavenging ROS and reactive nitrogen species (Carr and Frei, 1999; Kojo, 2004). The concentrations of NAC and AA used in this study were at a level shown to suppress the effects of ROS in previous studies (Carr and Frei, 1999; De la Fuente and Victor, 2001; Nakajima *et al.*, 2009).

Proliferative NSCs have a high endogenous ROS lev-

el (Le Belle *et al.*, 2011), and redox balance is important to regulate NSC/neural progenitor cell (NPC)-self-renewal and differentiation (Smith *et al.*, 2000; Li *et al.*, 2007; Hou *et al.*, 2012; Topchiy *et al.*, 2013). For example, mitochondrial superoxide negatively regulates NPC-self-renewal in the developmental cerebral cortex (Hou *et al.*, 2012). High levels of ROS inhibit O-2A progenitor proliferation (Smith *et al.*, 2000; Li *et al.*, 2007). In other cases, NADPH oxidase (Nox) 4-generated superoxide drives mouse NSC proliferation (Topchiy *et al.*, 2013). Ketamine-induced ROS enhanced the proliferation of NSCs derived from human embryonic stem cells (Bai *et al.*, 2013). The effect of ROS on NSC/NPC proliferation may change depending on the subcellular localization of the ROS generation and the timing of the ROS generation.

The suppression of NSC proliferation by the supernatants of both CNTs were virtually restored by the antioxidants, suggesting that the effects of CNT-supernatants were mediated through ROS stress. After a 5-hr sonication, multiple metals were detected in the SWCNT and MWCNT supernatants using ICP-MS. Mn, Rb, Cs, Tl, and Fe were detected in the SWCNT supernatant, and Mn, Cs, W, and Tl were detected in the MWCNT supernatant. Out of these SWCNT metals, the effects of Mn and Fe were reversed by antioxidants, suggesting that Mn and Fe play the main role in the suppression of NSC proliferation by CNT supernatants. In the MWCNT supernatant, the concentrations of Mn and Fe were insufficient to suppress NSC proliferation. Thus, a combination of ROS produced by multiple metals might produce synergistic suppressive effects.

Fe is essential for biological processes, but it is also known to be toxic in excess. Fe^{2+} overload into the cells and shuttling of Fe^{2+} to Fe^{3+} leads to cellular malfunctions due to ROS production (Halliwell and Gutteridge, 1992; Touati, 2000). Although Fe^{3+} has been largely considered as non-cytotoxic (Braun, 1997; Bruins *et al.*, 2000), it has its own mechanisms that can alter cell viability (Chamnongpol *et al.*, 2002). Fe^{3+} shows ROS production even while bound to proteins (Alekseenko *et al.*, 2008). GSH revealed pro-oxidant effects in the presence of an exogenous Fe^{3+} (Zager and Burkhart, 1998). Furthermore, Fe^{2+} and Fe^{3+} were shown to enter brain mitochondria and cause mitochondrial depolarization and ROS production (Sripetchwandee *et al.*, 2013). Mn is also essential for biological processes, but it has been known to be a neurotoxicant in excess. Mn induces oxidative stress (Choi *et al.*, 2007; Park and Park, 2010) and the release of cytokines (Park and Park, 2010). Mn further potentiates inflammation by the release of MMP9 through ROS production and modulation of ERK (Latronico *et al.*, 2013). Rb was also detected in the supernatants of SWCNT and MWCNT. Here, we found that Rb alone suppressed NSC proliferation in a ROS-independent manner. Rb has long been considered as nontoxic. Rb is generally used as a medical contrast medium because of its long half-life. Thus, the mechanism behind the Rb effects should be clarified quickly.

Most commercial CNTs contain ultrafine metal particles composed of Fe, Ni, Y, Co, Pb, and Cu that are used as catalysts (Ding *et al.*, 2008; Yazyev and Pasquarello, 2008; Banhart, 2009; Tyagi *et al.*, 2011). Recent studies showed that metal impurities play a major role in CNT cytotoxicity (Liu *et al.*, 2008; Kim *et al.*, 2010). The residual metals can remain in the contact solvent or embed inside the CNTs (Pumera, 2007; Fubini *et al.*, 2011; Aldieri *et al.*, 2013). In our study, the content of Fe in SWCNT was remarkable. A SWCNT is a graphene sheet protected metal core/shell of nanoparticles (Pumera, 2007). This structure may have caused the higher levels of metal impurities when compared with MWCNTs. Our data suggest that the residual metallic catalysts are released by vibration energy with a sonication frequency of 36 kHz, watt density of 65 W/264 cm^2 and sonication time of 5 hr. Pumera *et al.* indicated that washing with concentrated nitric acid removed up to 88% (w/w) of metal catalyst nanoparticles (Pumera, 2007). For public health and the safer applications of CNTs in nano-medicine, it is preferable to decrease the amount of the metal impurities by improving the washing process.

Conflict of interest---- The authors declare that there is no conflict of interest.

REFERENCES

Aldieri, E., Fenoglio, I., Cesano, F., Gazzano, E., Gulino, G., Scarano, D., Attanasio, A., Mazzucco, G., Ghigo, D. and Fubini, B. (2013): The role of iron impurities in the toxic effects exerted by short multiwalled carbon nanotubes (MWCNT) in murine alveolar macrophages. J. Toxicol. Environ. Health Part A, **76**, 1056-1071.

Alekseenko, A.V., Waseem, T.V. and Fedorovich, S.V. (2008): Ferritin, a protein containing iron nanoparticles, induces reactive oxygen species formation and inhibits glutamate uptake in rat brain synaptosomes. Brain Res., **1241**, 193-200.

Arfsten, D.P., Johnson, E.W., Wilfong, E.R., Jung, A.E. and Bobb, A.J. (2007): Distribution of radio-labeled N-Acetyl-L-Cysteine in Sprague-Dawley rats and its effect on glutathione metabolism following single and repeat dosing by oral gavage. Cutan. Ocul. Toxicol., **26**, 113-134.

Bai, X., Yan, Y., Canfield, S., Muravyeva, M.Y., Kikuchi, C., Zaja, I., Corbett, J.A. and Bosnjak, Z.J. (2013): Ketamine enhances human neural stem cell proliferation and induces neuronal apop-

tosis via reactive oxygen species-mediated mitochondrial pathway. Anesth. Analg., **116**, 869-880.

Balasubramanian, S.K., Poh, K.W., Ong, C.N., Kreyling, W.G., Ong, W.Y. and Yu, L.E. (2013): The effect of primary particle size on biodistribution of inhaled gold nano-agglomerates. Biomaterials, **34**, 5439-5452.

Banhart, F. (2009): Interactions between metals and carbon nanotubes: at the interface between old and new materials. Nanoscale, **1**, 201-213.

Belyanskaya, L., Weigel, S., Hirsch, C., Tobler, U., Krug, H.F. and Wick, P. (2009): Effects of carbon nanotubes on primary neurons and glial cells. Neurotoxicology, **30**, 702-711.

Braun, V. (1997): Avoidance of iron toxicity through regulation of bacterial iron transport. Biol. Chem., **378**, 779-786.

Bruins, M.R., Kapil, S. and Oehme, F.W. (2000): Microbial resistance to metals in the environment. Ecotoxicol. Environ. Saf., **45**, 198-207.

Carr, A. and Frei, B. (1999): Does vitamin C act as a pro-oxidant under physiological conditions? FASEB J., **13**, 1007-1024.

Caviness, V.S.Jr., Takahashi, T. and Nowakowski, R.S. (1995): Numbers, time and neocortical neuronogenesis: a general developmental and evolutionary model. Trends Neurosci., **18**, 379-383.

Chamnongpol, S., Dodson, W., Cromie, M.J., Harris, Z.L. and Groisman, E.A. (2002): Fe(III)-mediated cellular toxicity. Mol. Microbiol., **45**, 711-719.

Choi, C.J., Anantharam, V., Saetveit, N.J., Houk, R.S., Kanthasamy, A. and Kanthasamy, A.G. (2007): Normal cellular prion protein protects against manganese-induced oxidative stress and apoptotic cell death. Toxicol. Sci., **98**, 495-509.

Couillard-Despres, S., Iglseder, B. and Aigner, L. (2011): Neurogenesis, cellular plasticity and cognition: the impact of stem cells in the adult and aging brain--a mini-review. Gerontology, **57**, 559-564.

De la Fuente, M. and Victor, V.M. (2001): Ascorbic acid and N-acetylcysteine improve *in vitro* the function of lymphocytes from mice with endotoxin-induced oxidative stress. Free Radic. Res., **35**, 73-84.

Ding, F., Larsson, P., Larsson, J.A., Ahuja, R., Duan, H., Rosen, A. and Bolton, K. (2008): The importance of strong carbon-metal adhesion for catalytic nucleation of single-walled carbon nanotubes. Nano Lett., **8**, 463-468.

Donaldson, K., Poland, C.A., Murphy, F.A., MacFarlane, M., Chernova, T. and Schinwald, A. (2013): Pulmonary toxicity of carbon nanotubes and asbestos - similarities and differences. Adv. Drug Deliv. Rev., **65**, 2078-2086.

Eisch, A.J. and Petrik, D. (2012): Depression and hippocampal neurogenesis: a road to remission? Science, **338**, 72-75.

Ema, M., Matsuda, A., Kobayashi, N., Naya, M. and Nakanishi, J. (2011): Evaluation of dermal and eye irritation and skin sensitization due to carbon nanotubes. Regul.Toxicol. Pharmacol., **61**, 276-281.

Fubini, B., Fenoglio, I., Tomatis, M. and Turci, F. (2011): Effect of chemical composition and state of the surface on the toxic response to high aspect ratio nanomaterials. Nanomedicine (Lond), **6**, 899-920.

Gavello, D., Vandael, D.H., Cesa, R., Premoselli, F., Marcantoni, A., Cesano, F., Scarano, D., Fubini, B., Carbone, E., Fenoglio, I. and Carabelli, V. (2012): Altered excitability of cultured chromaffin cells following exposure to multi-walled carbon nanotubes. Nanotoxicology, **6**, 47-60.

Halliwell, B. and Gutteridge, J.M. (1992): Biologically relevant metal ion-dependent hydroxyl radical generation. An update. FEBS Lett., **307**, 108-112.

Hamanoue, M., Matsuzaki, Y., Sato, K., Okano, H.J., Shibata, S., Sato, I., Suzuki, S., Ogawara, M., Takamatsu, K. and Okano, H. (2009): Cell surface N-glycans mediated isolation of mouse neural stem cells. J. Neurochem., **110**, 1575-1584.

Henriksson, J. and Tjalve, H. (2000): Manganese taken up into the CNS via the olfactory pathway in rats affects astrocytes. Toxicol. Sci., **55**, 392-398.

Hou, Y., Ouyang, X., Wan, R., Cheng, H., Mattson, M.P. and Cheng, A. (2012): Mitochondrial superoxide production negatively regulates neural progenitor proliferation and cerebral cortical development. Stem Cells, **30**, 2535-2547.

Jaurand, M.C., Renier, A. and Daubriac, J. (2009): Mesothelioma: Do asbestos and carbon nanotubes pose the same health risk? Part. Fibre Toxicol., **6**, 16.

Kim, J.E., Lim, H.T., Minai-Tehrani, A., Kwon, J.T., Shin, J.Y., Woo, C.G., Choi, M., Baek, J., Jeong, D.H., Ha, Y.C., Chae, C.H., Song, K.S., Ahn, K.H., Lee, J.H., Sung, H.J., Yu, I.J., Beck, G.R.Jr. and Cho, M.H. (2010): Toxicity and clearance of intratracheally administered multiwalled carbon nanotubes from murine lung. J. Toxicol. Environ. Health Part A, **73**, 1530-1543.

Kim, K.K., Singh, R.K., Strongin, R.M., Moore, R.G., Brard, L. and Lange, T.S. (2011): Organometallic iron(III)-salophene exerts cytotoxic properties in neuroblastoma cells via MAPK activation and ROS generation. PloS One, **6**, e19049.

Kojo, S. (2004): Vitamin C: basic metabolism and its function as an index of oxidative stress. Curr. Med. Chem., **11**, 1041-1064.

Kriegstein, A. and Alvarez-Buylla, A. (2009): The glial nature of embryonic and adult neural stem cells. Ann. Rev. Neurosci., **32**, 149-184.

Latronico, T., Brana, M.T., Merra, E., Fasano, A., Di Bari, G., Casalino, E. and Liuzzi, G.M. (2013): Impact of manganese neurotoxicity on MMP-9 production and superoxide dismutase activity in rat primary astrocytes. Effect of resveratrol and therapeutical implications for the treatment of CNS diseases. Toxicol. Sci., **135**, 218-228.

Le Belle, J.E., Orozco, N.M., Paucar, A.A., Saxe, J.P., Mottahedeh, J., Pyle, A.D., Wu, H. and Kornblum, H.I. (2011): Proliferative neural stem cells have high endogenous ROS levels that regulate self-renewal and neurogenesis in a PI3K/Akt-dependant manner. Cell Stem Cell, **8**, 59-71.

Li, W., Nie, S., Yu, Q. and Xie, M. (2009): (-)-Epigallocatechin-3-gallate induces apoptosis of human hepatoma cells by mitochondrial pathways related to reactive oxygen species. J. Agric. Food Chem., **57**, 6685-6691.

Li, Z., Dong, T., Proschel, C. and Noble, M. (2007): Chemically diverse toxicants converge on Fyn and c-Cbl to disrupt precursor cell function. PLoS Biol., **5**, e35.

Liu, X., Guo, L., Morris, D., Kane, A.B. and Hurt, R.H. (2008): Targeted Removal of Bioavailable Metal as a Detoxification Strategy for Carbon Nanotubes. Carbon, **46**, 489-500.

Matsumoto, M., Serizawa, H., Sunaga, M., Kato, H., Takahashi, M., Hirata-Koizumi, M., Ono, A., Kamata, E. and Hirose, A. (2012): No toxicological effects on acute and repeated oral gavage doses of single-wall or multi-wall carbon nanotube in rats. J. Toxicol. Sci., **37**, 463-474.

Mistry, A., Stolnik, S. and Illum, L. (2009): Nanoparticles for direct nose-to-brain delivery of drugs. Int. J. Pharm., **379**, 146-157.

Nakajima, Y., Tsuruma, K., Shimazawa, M., Mishima, S. and Hara, H. (2009): Comparison of bee products based on assays of antioxidant capacities. BMC Complement. Altern. Med., **9**, 4.

Pacurari, M., Castranova, V. and Vallyathan, V. (2010): Single- and multi-wall carbon nanotubes versus asbestos: are the carbon nanotubes a new health risk to humans? J. Toxicol. Environ. Health A., **73**, 378-395.

Park, E.J. and Park, K. (2010): Induction of oxidative stress and inflammatory cytokines by manganese chloride in cultured T98G cells, human brain glioblastoma cell line. Toxicol. In Vitro, **24**, 472-479.

Persson, E., Henriksson, J. and Tjalve, H. (2003): Uptake of cobalt from the nasal mucosa into the brain via olfactory pathways in rats. Toxicol. Lett., **145**, 19-27.

Pumera, M. (2007): Carbon nanotubes contain residual metal catalyst nanoparticles even after washing with nitric acid at elevated temperature because these metal nanoparticles are sheathed by several graphene sheets. Langmuir, **23**, 6453-6458.

Reynolds, B.A., Tetzlaff, W. and Weiss, S. (1992): A multipotent EGF-responsive striatal embryonic progenitor cell produces neurons and astrocytes. J. Neurosci., **12**, 4565-4574.

Rolando, C. and Taylor, V. (2014): Neural stem cell of the hippocampus: development, physiology regulation, and dysfunction in disease. Curr Top Dev Biol., **107**, 183-206.

Roth, J.A. and Eichhorn, M. (2013): Down-regulation of LRRK2 in control and DAT transfected HEK cells increases manganese-induced oxidative stress and cell toxicity. Neurotoxicology, **37**, 100-107.

Sharma, H.S. and Sharma, A. (2007): Nanoparticles aggravate heat stress induced cognitive deficits, blood-brain barrier disruption, edema formation and brain pathology. Prog. Brain Res., **162**, 245-273.

Smith, J., Ladi, E., Mayer-Proschel, M. and Noble, M. (2000): Redox state is a central modulator of the balance between self-renewal and differentiation in a dividing glial precursor cell. Proceedings of the National Academy of Sciences of the United States of America, **97**, 10032-10037.

Sripetchwandee, J., Sanit, J., Chattipakorn, N. and Chattipakorn, S.C. (2013): Mitochondrial calcium uniporter blocker effectively prevents brain mitochondrial dysfunction caused by iron overload. Life Sci., **92**, 298-304.

Topchiy, E., Panzhinskiy, E., Griffin, W.S., Barger, S.W., Das, M. and Zawada, W.M. (2013): Nox4-generated superoxide drives angiotensin II-induced neural stem cell proliferation. Dev. Neurosci., **35**, 293-305.

Touati, D. (2000): Iron and oxidative stress in bacteria. Arch. Biochem. Biophys., **373**, 1-6.

Tyagi, P.K., Janowska, I., Cretu, O., Pham-Huu, C. and Banhart, F. (2011): Catalytic action of gold and copper crystals in the growth of carbon nanotubes. J. Nanosci. Nanotechnol., **11**, 3609-3615.

Xu, L.J., Zhao, J.X., Zhang, T., Ren, G.G. and Yang, Z. (2009): *In vitro* study on influence of nano particles of CuO on CA1 pyramidal neurons of rat hippocampus potassium currents. Environ. Toxicol., **24**, 211-217.

Yazyev, O.V. and Pasquarello, A. (2008): Effect of metal elements in catalytic growth of carbon nanotubes. Phys. Rev. Lett., **100**, 156102.

Yim, M.B., Chae, H.Z., Rhee, S.G., Chock, P.B. and Stadtman, E.R. (1994): On the protective mechanism of the thiol-specific antioxidant enzyme against the oxidative damage of biomacromolecules. J. Biol. Chem., **269**, 1621-1626.

Zager, R.A. and Burkhart, K.M. (1998): Differential effects of glutathione and cysteine on Fe2+, Fe3+, H2O2 and myoglobin-induced proximal tubular cell attack. Kidney Int., **53**, 1661-1672.

Zhang, Z., Teruya, K., Eto, H. and Shirahata, S. (2011): Fucoidan extract induces apoptosis in MCF-7 cells via a mechanism involving the ROS-dependent JNK activation and mitochondria-mediated pathways. PloS One, **6**, e27441.